CERN/DRDC/91-21
DRDC/P5-Add.1
13th March, 1991

HADRONIC AND ELECTROMAGNETIC LIQUID ARGON LHC PROTOTYPE CALORIMETER WITH POINTING GEOMETRY

B. Aubert, A. Bazan, B. Beaugiraud, J. Colas, M. Lebeau, T. Leflour, J.C. LeMarec, M. Maire, P. Petitpas, J. Thion, J.P. Vialle, I. Wingerter-Seez
LAPP, Annecy, France

H.A. Gordon, V Radeka, D. Rahm, D. Stephani
Brookhaven National Laboratory, Upton, USA

J.L. Chevalley, C.W. Fabjan[2)], A. Franz, P. Farthouat, O. Gildemeister, P. Jenni, M. Lefebvre*, M. Nessi, F. Nessi-Tedaldi, M. Pepe, W. Richter, G.R. Stevenson, W.J. Willis
CERN, Geneva, Switzerland

J.M. Baze, L. Gosset, P. Lavocat, B. Mansoulie, J.P. Meyer, J.F. Renardy, J. Teiger, H. Zaccone
DPhPe-CEN Saclay, Gif-sur-Yvette, France

C. Battistoni, D. Camin, D. Cavalli, G. Costa, A. Ferrari, F. Gianotti, L. Mandelli, M. Mazzanti, L. Perini
Dipartimento di Fisica dell'Università e Sezione INFN, Milano, Italy

E. Augé, R.L. Chase, J.C. Chollet, C. de la Taille, L. Fayard, D. Fournier[1)], G. Guilhem, A. Hrisoho, L. Iconomidou-Fayard, Ph. Jean, B. Merkel, J.M. Noppe, G. Parrour, P. Pétroff, J.P. Repellin, A. Schaffer, N. Seguin, J.J. Veillet
LAL, Orsay, France

C. Fuglesang
Manne Siegbahn Institute, Stockholm, Sweden

ABSTRACT:

The design and cost evaluation of a hadronic and electromagnetic prototype calorimeter is presented. This design follows the main ideas described in the Proposal. New studies have been made concerning a mechanical evaluation of a full liquid argon calorimeter, a comparison of lead and iron as converter materials for the hadronic part, and a full simulation of the pointing geometry.

(1) Spokesman
(2) Contactman
* Now at University of Victoria, BC, Canada

1. INTRODUCTION:

Since the Proposal [1] was submitted, we have been working on the following topics:

1. Analysis of the test beam data taken in 1990
2. Development and construction of fast shapers.
3. Study of new preamplifier concepts, improvement of the previously used GaAs and Si hybrids.
4. Simulation of radiation levels in a cylindrical calorimeter geometry.
5. Mechanical study of a full electromagnetic and hadronic calorimeter. Cryostat studies.
6. Simulation of pion and jet showers.
7. Optimisation of the parameters for an electromagnetic calorimeter with pointing geometry.
8. Design of a hadronic and electromagnetic prototype.
9. Design of a facility for radiation tests in liquid argon.

Concerning point 1, we attach to the present Addendum, a preliminary version of the paper we intend to submit to NIM [2]. New electronics (points 2 and 3) has been developed following the Proposal and will be used in the 1991 beam tests which we are now preparing. Points 5, 6, 7 and 8 are the main topics of the present Addendum. Some results on point 4 (radiation levels) will be presented (chapter 5), as they are relevant for converter material comparisons for the hadronic calorimeter.

In order to get to the stage where a design of a prototype, useful for the evaluation of the technique as an LHC calorimeter candidate, could be made, we have found it necessary to first make a preliminary study of a full LHC calorimeter.

This study required that the basic working options be known. We have maintained the 'accordion' geometry, and the electrostatic transformer readout –EST– (in the hadronic part) as presented in the Proposal. Further steps required a knowledge of the converter material. This important choice –between iron or copper, and lead– was made after the analysis of detailed simulations. A summary of this work is presented in chapter 2, followed by the optimisation of parameters for the electromagnetic section.

In chapter 3, we outline the results of a general "pre–study" for an LHC calorimeter, while section 4 is devoted to the prototype design and its cost evaluation.

2. SIMULATIONS

2.1 Simulations of Hadronic showers.

Since the Proposal, several studies have been performed.

For testing purposes, we ascertained that GEANT 3.14 interfaced to GHEISHA for the hadronic response, reproduces well existing LAr calorimeter results. In particular, the 1986 H1 prototype data [3] (lead liquid argon electromagnetic section, followed by a copper liquid argon hadronic section) were used, and experimental results for hadron and jet resolution and e/π response ratios were reproduced within 10%.

A full simulation of a calorimeter consisting of an electromagnetic and hadronic section, both with an accordion structure, was developed. For the electromagnetic part, the geometrical parameters (thicknesses, 'accordion'–fold pitch) were chosen to be similar to those of the prototype calorimeter exposed to a test beam in 1990 [2]. For the hadronic section, 1 cm thick plates and 2 mm LAr gaps were used. The bending angle was 45^{o}, the accordion fold 28.8 cm, and a total thickness of 160 cm corresponded to 8 interaction lengths. To speed up the simulations, sharp corners were assumed for both calorimeter compartments. The transverse dimensions of the calorimeter were chosen so as to fully contain the showers. Dead material representing a cryostat in front and mechanical supports between the electromagnetic and hadronic sections, were included in the simulation.

With these calorimeter definitions, different studies of resolution and shape of the reconstructed energy spectrum were performed, using mostly 150 GeV PYTHIA jets, and collecting typically 1000 events in each condition. An intercalibration between the electromagnetic and the hadronic sections was applied through a unique calibration factor, chosen to equalize the response in both compartments. A first attempt to improve further the overall response with an increased number of parameters in this equalization is described below.

The difference between accordion geometry and planar parallel electrodes was first studied (the results for the latter one can be found in the original Proposal). If one compares equivalent samplings, no significant difference within statistics is observed in the resolution that can be achieved with either geometries.

Lead and Iron were investigated as possible candidates for the showering material in the hadronic section. We observed a typically 10% better resolution when Lead was used. Part of this difference can be associated to smaller tails in the energy response with Lead. These are mainly produced by events where almost all the energy is deposited in the hadronic section. However, an improvement might be achieved using a more refined intercalibration.

As we know from studies of other non–compensating calorimeters (for example in CDHS, NA31, H1), it is possible with sufficient granularity to improve substantially the energy resolution (while maintaining adequate linearity) by using energy or position dependent weights. At LHC, one has to be particularly careful in the choice of weights in order not to increase the pileup effect.

In a first attempt, the calorimeter was divided in three EM (Pb/LAr) and four hadronic (Fe/LAr) longitudinal compartments, to which (linear) energy dependent weights were assigned:

$$\alpha_i = A_i + B_i E_i$$

where E_i is the energy deposited in the i–th compartment. The 14 coefficients were determined by minimizing the spread of the total measured energy. In Fig. 1., a comparison of the resolution with and without weighting is shown for 150 GeV jets. The energy resolution using this simple method improves from 6.1 ± 0.3 % to 4.5 ± 0.2 %. A similar behaviour was observed for simulated charged pions with energies between 30 and 150 GeV. This initial study already demonstrates that, with the chosen granularity, there is indeed room for a sizeable improvement with weights. However, the evaluation of this technique requires a dedicated study which we are just starting now.

2.2 Simulation of an electromagnetic calorimeter with pointing geometry

Simulations of electromagnetic showers in the 'accordion' structure have been one of the main tools in defining the parameters of the prototype tested in 1990 [1]. Comparison of the simulation with electron and muon data, has shown good agreement. In particular a modulation of the energy response (at a level slightly below one percent), as a function of electron impact with respect to 'accordion' folds, is present at the expected level [2]. For these comparisons, the various layers of converter cladding and readout electrodes were introduced in the GEANT simulation.

For more flexibility in detector optimisation, we have found it convenient to use, in addition to full electron shower simulations, a geometrical calculation of thicknesses of various materials along a straight line going through the calorimeter. This is done in GEANT using non interacting particles called "geantinos". Such geometrical thicknesses, when weighted by the longitudinal profile of a shower, give an indication of the material thicknesses actually experienced by the shower. Both approaches were used to study and optimise the two pointing geometries which we are considering (see chapter 4). The aim is to find and optimise a geometry, derived from the one used in the test, where pointing towers of typically $\Delta\phi \times \Delta\eta = 0.02 \times 0.02$ span the whole calorimeter from pseudo–rapidity −1.7 to +1.7 without any crack in azimuth.

In the first configuration, called "constant angle geometry", one would use the same electrode geometry as for the test, with a constant fold angle of 90^o, but this time disposing them radially around the axis of the calorimeter. In this case the sampling fraction increases with depth. Also, the relationship between the length of the 'accordion' fold and the electrode pitch [1] can only be satisfied at a given depth, chosen to be the shower maximum. To overcome the change in the sampling fraction, which also depends upon the shaping time, one can either reduce the argon gap by increasing the amount of epoxy–glass in the electrodes with depth, or (and) weigh differently the energy measured in the front and back sections. Simulations performed at 40 GeV and 100 GeV have shown a resolution close to the one obtained with the same electrodes arranged parallel to each other. It was thought, however, that this finding requires confirmation in a beam test. This will be done this summer, using a newly built prototype of a size similar to the one used in 1990 (40 x 40 cm^2 front face).

To get the best possible performance, a second solution uses electrodes for which the folds inscribe themselves in a cone pointing to the vertex (Fig 2). In this case, a 'constant liquid argon gap', and therefore a constant sampling fraction, is obtained by varying the fold angle with depth. Also the relationship between argon gap and 'accordion' fold, which minimizes the residual modulation of response with position [1], can be satisfied at all depths. To optimise the parameters, we used the two above mentioned approaches. The inner radius of the calorimeter, and the number of (radial) plates around the calorimeter, were chosen first, and the 'accordion' fold length and angle (at one depth) were varied around values close to the ones used for the 1990 beam test prototype. Figure 3 shows the variation of argon thickness, with azimuth, when the impact of the "geantino" goes from an outbending corner of the kapton electrode (−0.5) to the next (+0.5). The thickness is weighted with longitudinal profiles of electrons of 5 GeV, 30 GeV and 100 GeV respectively. Figure 4 displays the energy response to electron showers of a corresponding energy as a function of azimuth. The spread from the shower simulation is indeed smaller than the geometrical estimation, due to the averaging associated to the shower transverse size. When compared to similar distributions for parallel 'accordion' electrodes, shown in Fig. 16 of the Proposal, we see that about the same performances are expected from a detector with pointing geometry, when compared to the prototype with parallel 'accordion' electrodes, already tested [2].

The difficulty in building such a detector, with the required tolerances, is addressed in the next chapter.

3. STUDY OF A FULL LIQUID ARGON CALORIMETER FOR AN LHC EXPERIMENT

3.1 General architecture.

In our mechanical design, based on the 'accordion' geometry and EST readout in the hadronic section, the hadronic and electromagnetic calorimeters are two coaxial shells, in which modules are hooked onto an outer cylinder reinforced by washers. For the hadronic part, this role is played by the cold vessel. For the electromagnetic part, a thin structural cylinder plays this role. It is supported by the cold vessel on 6 points: 2 at the level of the central washer and 2 at each end.

Taking advantage of the 'accordion' shape, both calorimeters offer complete azimuthal symmetry without cracks. Along the beam direction there is a single crack at $\eta = 0$. In both calorimeters, readout is organized in towers pointing to the vertex in both azimuth and rapidity. The mechanical parameters have been adjusted in such a way that 2 hadronic towers overlap 5 electromagnetic towers, in both directions. Two options are considered for the electromagnetic part: 'constant gap' and 'constant angle'.

A preliminary study has been made to accommodate the design of the calorimeter stacks, while minimizing the amount of dead material. The problem is particularly critical in the region between the barrel and end–cap parts of the calorimeter. Indeed, preliminary calculations show that the use of flat walls would lead to unacceptable wall thicknesses, and that the use of bulgy walls would lead to unacceptable cracks and loss of space. Therefore we have tried to find a design where most of the wall effects are taken by the structure which already bears the main load.

Two solutions were brought forward in this spirit :

In the first one (Fig. 5) the end–cap is secured to the barrel and the thin walls lean against each other. The walls are cold, and the heat losses to the exterior are limited by an intermediate vacuum independent of the vacua of the barrel and of the end–cap. Thermally non–conducting sheets provide the separations of the vacua. In this design, the pressures in the barrel and in the end–cap have to be balanced; thus the barrel and end–caps cryostats must be filled (and emptied) at the same time, and must have a common gas exhaust. In particular, the whole calorimeter must be emptied before recessing an end–cap. Note, however, that it can be kept cold: contrarily to the cooling down time, emptying or filling with liquid can be quite short.

In the second, more classical one (Fig.6), we take into account the fact that, in the previous design, it was mechanically difficult to manage the cool down of the ends of the vacuum enclosures. Indeed large stresses are generated if the inner and outer boundaries of the end wall are at ambiant temperature and the centre of the same wall is at liquid argon temperatue. It is then proposed to have, on each side, a cryostat structure with a double wall, and with spacers between the two walls in order to transfer the efforts. In this design, the cold end wall of the argon vessel is tied to the calorimeter modules. The hydrostatic pressure of the liquid is then taken up as a traction on the modules. This approach is well suited for our module geometries (see below) where 'accordion' shaped plates, parallel to the beam axis, can take large forces. The warm wall is separated from the cold wall by vacuum, except at a few points where insulating spacers hold the gap. In this design the barrel and end–cap cryostats are independent as in a classical solution.

The vacuum and argon vessels are made of 8m long stainless steel cylinders. The rigidity of the cold vessel is largely given by three washers: a central one, single pieced, and two end–flanges which can be dismounted by sectors for module installation. Three outer rings are also part of this structure. It has been estimated that 35 mm is a possible figure for the cold and warm outer walls. For the inner walls, several options are being considered to reduce the thickness down to 0.5 radiation lengths or below (aluminum walls, corrugated stainless steel walls, tying the argon wall to the internal structure, etc.). Cables from the calorimeter exit the vessels at both ends of the barrel with feed–throughs. The gas exhausts are also in this region. The pumping and feeding pipes for the liquid are located at the bottom. The vacuum vessel is supported by 6 legs. Each ring of the argon vessel is supported by two insulating legs (located inside the legs of the vacuum vessel) which ensure the relative displacements due to thermal contraction.

3.2 Hadronic calorimeter.

Since the Proposal, simulation and design studies resulted in a better definition of the hadronic calorimeter. While the working option had first been lead, we decided to turn to iron which is better for the following reasons. First, iron provide a better mechanical rigidity, secondly, for the same 8λ the total weight is reduced by almost 30%, thirdly, the multiple scattering for the muons identified outside the hadron calorimeter is reduced by a factor larger than $\sqrt{2}$, and finally the neutron fluence is smaller (see section 5.1). The energy resolution (see section 2.1) is indeed better with Lead, but we think the ~ 10% better figure does not outweigh the other arguments. We have seen no advantage to copper over iron.

The cell sizes have been tuned to 0.049 x 0.046, to match the electromagnetic granularity. The smaller size compared to the Proposal (0.06 x 0.06) give a gain of close to ($\sqrt{2}$) on the signal to noise ratio. A further improvement in the noise is due to a change in the sampling ratio in the last two samplings in depth where in the pointing geometry the cell dimensions become large. The ratio iron/liquid Argon will be 10/3, whreas it is 10/2 in the first two samplings. The full hadronic calorimeter is build longitudinally in two halves , each of them divided into 32 azimuthal sectors (see Fig. 7). The dimensions of the sector are: length 4 m, inner/outer diameter of the active part 2 m/3.8 m. The sector covers an azimuth size of $2\pi/32$ divided into 4 slices of $2\pi/128$. In the radial direction, it is divided into an inner module with two samplings in depth (3 λ), and an outer module with two sampling (5 λ) separated by a space for cables and preamplifiers. Each of these modules is a stack made of 'accordion'–shaped plates of different types (Figs. 8 and 9):

– ground plates: all stainless steel, which have two purposes : one mechanical as a support structure and one electrical as a ground structure. There are three 10 mm thick ground plates inside the module between the 4 azimuthal slices, and two 5 mm thick plates on the sides of the sector. As two sectors are joint together, the two adjacent ground plates give the same absorber thickness as the inner ground plates of 10mm.

– electrode plates : 10 mm thick stainless steel plates which have been cut and reassembled between two fiberglass sheets into a composite plate. Copper pads are included in the process for charge collection and transport. Cuts along the folds of the 'accordion' provide separate samplings in depth, while cuts across the folds provide the rapidity segmentation of the module, following a pointing geometry.

Each element is electrically insulated from its neighbours by insulating shims. These composite plates are stacked between two ground plates with equal gaps between all plates. In the inner module, 5 composite plates provide 6 argon gaps, in the outer module 7 plates provide 8 argon gaps, giving EST ratios of 3 and 4 respectively.

3.3 Electromagnetic calorimeter

For the Electromagnetic calorimeter, we plan to follow techniques adapted and improved from the ones used in the prototype test [1, 2]. Main modifications follow the implications of achieving a full azimuthal symmetry, with no cracks, with readout organised in towers pointing to the vertex.

The working dimensions are those already mentioned in the simulation section, the inner radius of the active part starting at 1350 mm. The azimuth is covered by 960 radial plates. Readout towers are defined by strips chemically etched on readout kapton electrodes. Three such strips are connected together to define the readout pitch in phi, which is thus $2\pi/320 = 0.0197$. In the other direction the strip shape is defined to cover equal rapidity intervals. Choosing 0.01764 for this interval corresponds to 96 electronic channels along the 4m length of the calorimeter (with the outermost corner truncated at 3.6 m), for a rapidity interval from 0 to 1.7 (polar angle θ from 90 to 21°). At large rapidities, the incidence angle on the converter electrodes becomes small, worsening somewhat the expected resolution (in $\Delta E/E$, like $1/\sqrt{\sin\theta}$). For the same reason, the actual thickness of the calorimeter, seen from the vertex, becomes much too large. To overcome this problem, our proposal is to change the structure of the Lead–stainless steel converter electrodes at rapidities $\pm$ 0.55 and $\pm$ 1.1. A sketch of this is shown in Fig. 10. We have verified with shower simulations (see section 2.2) that this change does not imply an important broadening (less than 20%) of the shower transverse size. As previously discussed, a good uniformity of energy response as a function of azimuth, requires that the electrode shape follow closely the calculated profile (see Fig. 2), and that the relative positioning of these electrodes be accurate enough. We estimate that the positioning in azimuth should be made with a systematic 'scale uncertainty' smaller than 0.5 percent (0.04 mm with respect to the 8 mm pitch of electrodes around the inner calorimeter cylinder), and that rare local imperfections up to 0.2 mm are tolerable. As for the hadronic calorimeter, we plan to divide the electromagnetic part into modules (40 modules, each covering 9° in azimuth) with a division in 2 along the beam direction. Our present ideas on the mounting of the modules into the support cylinder are depicted in Fig. 11. The assembly of modules in the cylinder would be done vertically. Once positioned in the cylinder, the active part of the calorimeter should be seen uniform, irrespective of module frontiers. This difficult problem requires a dedicated study which we have just started.

A module consists of 24 converter plates and 24 kapton readout electrodes (see Figs. 12 and 13). The plates are supported along their periphery. Along edges parallel to the beam, the converter plates are glued into precision machined bars with a groove (see Fig. 14). Windows in the bars allow signals from the kapton electrodes to get out. Each bar is precisely positioned to the next with pins. The module is tied by (curved) bolts every 10 cm. For reasons of transparency, the front bars are made of fiberglass–epoxy (with a suitably chosen composition to get an expansion coefficient close to that of the electrodes). The rear bars are in stainless steel. Owing to the composite nature of the converter electrodes, it is not fully granted that, after cooling cycles, electrodes in the horizontal plane will not take a sagitta larger than our tolerances (see above). Mechanical tests will be performed to assess this question. In the end, an uniformity scan of a prototype calorimeter of a size large enough, and incorporating frontiers between modules, will be the final proof. This is an important part of the test programme that we describe below (section 5).

As an alternative to the mechanical structure described above, one can use converter plates with a constant fold angle (90^o) (see section 2.3 for implications of this choice on expected performances). In this case the accordion folds need not be parallel to the cylinder axis. A favourable solution consists in choosing a tilt angle of 35^o, such that the folds are now perpendicular to the particles entering the calorimeter modules at the mid–acceptance point ($\theta = 55^o$). The main advantage of this solution is that now the accordion folds participate to the inertia of the plate (against the effects of their weight), strongly preventing a sagging of horizontal plates (see Fig. 15). Similar concepts to those described above can be applied to bind the modules, with the required accuracy, into the support cylinder (see Fig. 16). Due to the 'wavy' edges all around the modules, the construction of the modules would, however, rely on a different approach to the one using bars.

In the two approaches the kapton readout electrodes are positioned in between the converter electrodes using light honeycomb [1,2]. These elements do not participate in the overall rigidity of a module.

As in the pre–prototype [1,2], preamplifiers will be placed as close as possible to the kapton electrodes. The complete design of the mother boards and calibration boards will proceed with the preparation of the 1992 prototype (see section 4).

4. PROTOTYPE OF A HADRONIC AND ELECTROMAGNETIC CALORIMETER

Following this preliminary study of a calorimeter for LHC, we would like to conduct a series of beam tests to confirm the validity of our choices, and demonstrate adequate performances for LHC.

In order to be as specific as possible, the prototype we are proposing is a calorimeter primarily defined as a sector in rapidity and azimuth of the barrel calorimeter described in section 3.

To fully contain a hadronic (pion) shower, with some flexibility for a (reduced) scan, and to allow for some measurement of 'pseudo jets' produced by interactions in a plastic target, we are designing the prototype to cover 22.5^o in azimuth, and a rapidity interval from 0.0 to 0.5.

For the electromagnetic section, we choose as first option the 'constant gap' solution. In order to be most sensitive to potential sagging effects on the converter electrodes (see above), we need an electrode length much larger than the calorimeter depth. However, to limit construction expenses and delays, we restrict ourselves to 2 meters. The central rapidity region, where the Lead thickness is maximum, (see Fig. 10) is also the most sensitive area in this respect. Furthermore, we will place the module in the horizontal position, where gravity has the larger effects.

A schematics of the geometry of the prototype, following these criteria, is shown in Fig 17. In order to limit the test cryostat size, (see Fig. 18) we propose to remove the last folds of the hadronic part, thus limiting the total thickness to 7 interaction lengths, still acceptable at SPS energies.

The total number of readout channels in this calorimeter is about 3500. To aim at a full scan, most of them will have to be equipped with preamplifiers. For the shapers and subsequent parts (ADC), outside the cryostat, a set of 1000 channels is adequate. The necessary electronics is being developed by our collaboration, and will be tested (fast shapers) during the 1991 beam period using the 'old' electromagnetic prototype [1,2], and the one now built to test the constant angle solution (see section 2.2).

Following the construction techniques described in section 3, we have estimated the cost and time to build this calorimeter prototype. They are given in Tables 1 and 2. The figures given assume that adequate manpower will be available in the collaborating institutes.

In case the test should demonstrate mechanical problems beyond the acceptable level (uniformity worse than 0.5%), with the chosen electromagnetic calorimeter solution, one would turn to the 'constant angle', 35^{o} solution, which will be tested (on a small scale) this summer. In that case it would be sufficient to build an electromagnetic section just matched in dimension to the hadronic one. The cost estimate given in Table 1 assumes that tooling for the first solution will be designed, as far as possible, to be easily adapted to the second one.

Concerning the cryostat, we have found no available device that could meet fully our needs. We have therefore estimated the cost and time to build (in industry) a simple foam insulated cryostat. This is also given in Tables 1 and 2.

To cover the expected expenses, the estimated cost is 2330 kCHF, of which 300 kCHF correspond to the second electromagnetic option. This amount, not even counting this last item, is somewhat larger than our planned resources for this project: 1750 kCHF*.

A solution to this problem might come from contacts we presently have with other groups. In case we are not successful in that direction, we have considered using the H1 cryostat, which would save us about 150 kCHF. This cryostat, which is likely to be free in the second half of 1992, has a useful diameter (2500 mm) able to accommodate our prototype calorimeter, though in the vertical direction. Despite the fact that this would seriously limit the outcome of the test, we are keeping contacts with the H1 collaboration.

---

*This does not include the BNL contribution for 1992, which is presently under discussion.

5. RADIATION

5.1 Simulation of radiation levels

As a continuation of the work already described in the Proposal, the radiation level estimate in a cylindrical calorimeter was pursued. Present simulations predict neutron fluences up to a factor 10 larger in the low rapidity regions than previously estimated [4,5]. The reasons for this effect have been extensively investigated and are believed to rely on a larger albedo fluence than the one used in [4] and in the effect of neutron multiple scatterings inside the cavity. Detailed descriptions of the calculations will be given elsewhere [6]. The main interest here is to show the difference in neutron fluences at different points in the calorimeter and in the cavity, in the hypothesis that the hadronic calorimeter material is either Lead or iron. The geometry used is shown in Fig. 19, and the results obtained at different test points (1 to 17, see figure) are given in Table 3. The two columns to the right refer to numbers obtained when a moderator of 10 cm polyethylene is between the front face of the calorimeter and a 'preshower' including 1.5 rad length of Lead. The benefit of going from Lead to iron ranges from 30% in the low fluence region to a factor 2 in the highly exposed points, and is somewhat lower than sometimes anticipated [5]. This relies on the fact that most low energy hadrons deposit a large fraction of their energy in the (Lead) electromagnetic section. To elaborate on this point, we plan to introduce in the simulation the more complex structure of the electromagnetic converter plates that we have now in mind (Fig. 10), where at rapidities greater than 0.55 a sizeable fraction of the Lead is replaced by iron.

5.2 A facility for radiation exposures in liquid argon

As stressed in the Proposal, progress has already been achieved to strengthen the only weak element of a liquid argon calorimeter, the preamplifiers, against radiation damage. In order to be able to test the various preamplifiers in working conditions, we have designed a small size cryostat, to be operated close to the positron target of the Orsay Linac, where the estimated flux of neutrons (above 1 MeV) [7] is about 1.5 10^{13} neutrons/cm^2/hour. A sketch of the installation is shown in Fig. 20. The cryostat will be operated with liquid argon. Enough feed–throughs should allow to test up to 50 preamplifier channels at a time. Radioactive sources will allow pollution estimates from various materials exposed to radiations. The estimated cost of the installation is about 70 kCHF (already taken into account when estimating our resources for the 1992 Calorimeter prototype). It should be fully operational in early 1992.

6. CONCLUSION

The concept of a high granularity liquid argon electromagnetic calorimeter based on the 'accordion' geometry, has been successfully tested in 1990 using a 'pre–prototype'. The studies will continue in 1991 with faster electronics.

Simulations and mechanical studies have demonstrated that this approach could be extended, with pointing geometry, to a full LHC calorimeter. Similar studies have shown that this geometry, coupled with electrostatic transformer readout is also well suited to hadronic calorimetry. Preliminary attempts to design a full cryostat system indicate that new solutions can be found to improve the hermiticity of a liquid argon system, compared to previous approaches. To confirm these findings by beam tests, we propose to build a prototype sector of this preliminary view of an LHC calorimeter.

References

[1] Proposal 'Liquid Argon Calorimetry with LHC Performance Specifications', B. Aubert et al., CERN/DRDC/90–31, DRDC/P5

[2] Performance of a Liquid Argon electromagnetic calorimeter with 'accordion' geometry, B. Aubert et al. To be submitted to Nucl. Inst. and Methods.

[3] H1 Collaboration, W. Braunschweig et al., Nucl. Instr. Meth. A 265, (1988) 419 and Nucl. Instr. Meth. A 275, (1989) 246. H1 Collaboration, to be published in Proc. XXV Int. Conf. on High Energy Physics, Singapore (1990), Eds. K.K.Phua and Y. Yamaguchi.

[4] D.E. Groom (ed) 'Report on the task force group on radiation levels in the SSC interaction regions'. SSC Central Design Group report SSC–SR–1033 (1988).

[5] G.R. Stevenson 'New dose calculations for LHC Detectors'. Proceedings of the LHC workshop, Aachen 1990, Report CERN 90–10/ECFA 90–133 Vol. 3 (1990) p. 566.

[6] A.Ferrari and G.R.Stevenson, Internal note

[7] B.Merkel: Proceedings of the LHC workshop, Aachen 1990, Report CERN 90–10/ECFA 90–133 vol 3 (1990) p. 596.

Tables

Figure Captions

Table 1

Electromagnetic: Tooling Electromagnetic: components	300 320
Hadronic:	700
Cryostat:	165
Platform for beam test:	30
Cables and feedthroughs:	100
Preamplifiers:	150
Shapers:	80
	1845
10% contingency	185
	2030 kCHF
Electromagnetic, 'constant angle'	300
	2330 kCHF

	1.4.91	1.7.91	1.10.91	1.1.92	1.4.92	1.7.92
ELECTROMAGNETIC						
Tooling : design	↔	↔				
Tooling: manufacture – test	↔	↔	↔			
Components: delivery and test			↔			
Plate production				↔		
Assembly, test of modules				↔	↔	
Installation					↔	
HADRONIC						
Design	→					
Components: delivery and test	↔	↔				
Tooling: test		↔				
Plate production			↔			
Assembly, test of modules				↔	↔	
Transport to CERN installation					↔	
Calorimeter in beam						←
CRYOSTAT						
Design	→					
Construction		↔	↔	↔		

Table 2

Table 3: Integrated neutron flux per year of operation, assuming T_{beam} = 1 x 10^7s yr^{-1}, L = 1 x 30^{34} s^{-1} cm^{-2}, sig. = 60 mb

Position	<η>	Flux (n cm^{-2} yr^{-1}), En > 100 KeV			
		Pb–LAr without mod.	Fe–LAr without mod.	Pb–LAr with mod.	Fe–LAr with mod.
Barrel					
1: Preshower	0.0	1.6 x 10^{13}	1.2 x 10^{13}	2.7 x 10^{12}	1.7 x 10^{12}
2: Preshower	1.2	1.8 x 10^{13}	1.4 x 10^{13}	4.0 x 10^{12}	2.1 x [illegible]
3: Preshower	1.7	2.9 x 10^{13}	2.0 x 10^{13}	5.8 x 10^{12}	3.2 x 10^{12}
4. EM LAr entrance	0.0	8.7 x 10^{12}	7.3 x 10^{12}	3.2 x 10^{12}	3.1 x 10^{12}
5: EM LAr entrance	0.9	1.0 x 10^{13}	8.5 x 10^{12}	3.6 x 10^{12}	3.6 x 10^{12}
6: EM LAr entrance	1.5	1.5 x 10^{13}	1.2 x 10^{13}	4.3 x 10^{12}	4.2 x 10^{12}
7: EM LAr exit	0.0	5.7 x 10^{12}	4.3 x 10^{12}	3.2 x 10^{12}	3.0 x 10^{12}
8: EM LAr exit	0.7	6.5 x 10^{12}	5.1 x 10^{12}	3.6 x 10^{12}	3.0 x 10^{12}
9: EM LAr exit	1.3	8.0 x 10^{12}	6.9 x 10^{12}	4.5 x 10^{12}	3.5 x 10^{12}
End Cap :					
10: Preshower	2.6	5.7 x 10^{13}	3.7 x 10^{13}	1.8 x 10^{13}	1.0 x 10^{13}
11: Preshower	2.1	2.8 x 10^{13}	2.0 x 10^{13}	2.8 x 10^{12}	1.8 x 10^{12}
12: EM LAr R = 45	2.9	1.5 x 10^{14}	1.1 x 10^{14}	1.4 x 10^{14}	8.8 x 1[illegible]
13: EM LAr R = 178	1.6	1.8 x 10^{14}	7.8 x 10^{13}	1.2 x 10^{14}	6.4 x 10^{13}
14: EM LAr entrance	2.3	7.5 x 10^{13}	5.4 x 10^{13}	5.4 x 10^{13}	4.2 x 10^{13}
15: EM LAr exit	2.4	1.4 x 10^{14}	7.6 x 10^{13}	1.2 x 10^{14}	7 x 10^{13}
16: EM LAr entrance	1.7	2.9 x 10^{13}	1.6 x 10^{13}	1.7 x 10^{13}	1.3 x 10[illegible]
17: EM LAr exit	1.8	4.3 x 10^{13}	1.8 x 10^{13}	3.2 x 10^{13}	1.6 x 10^{13}

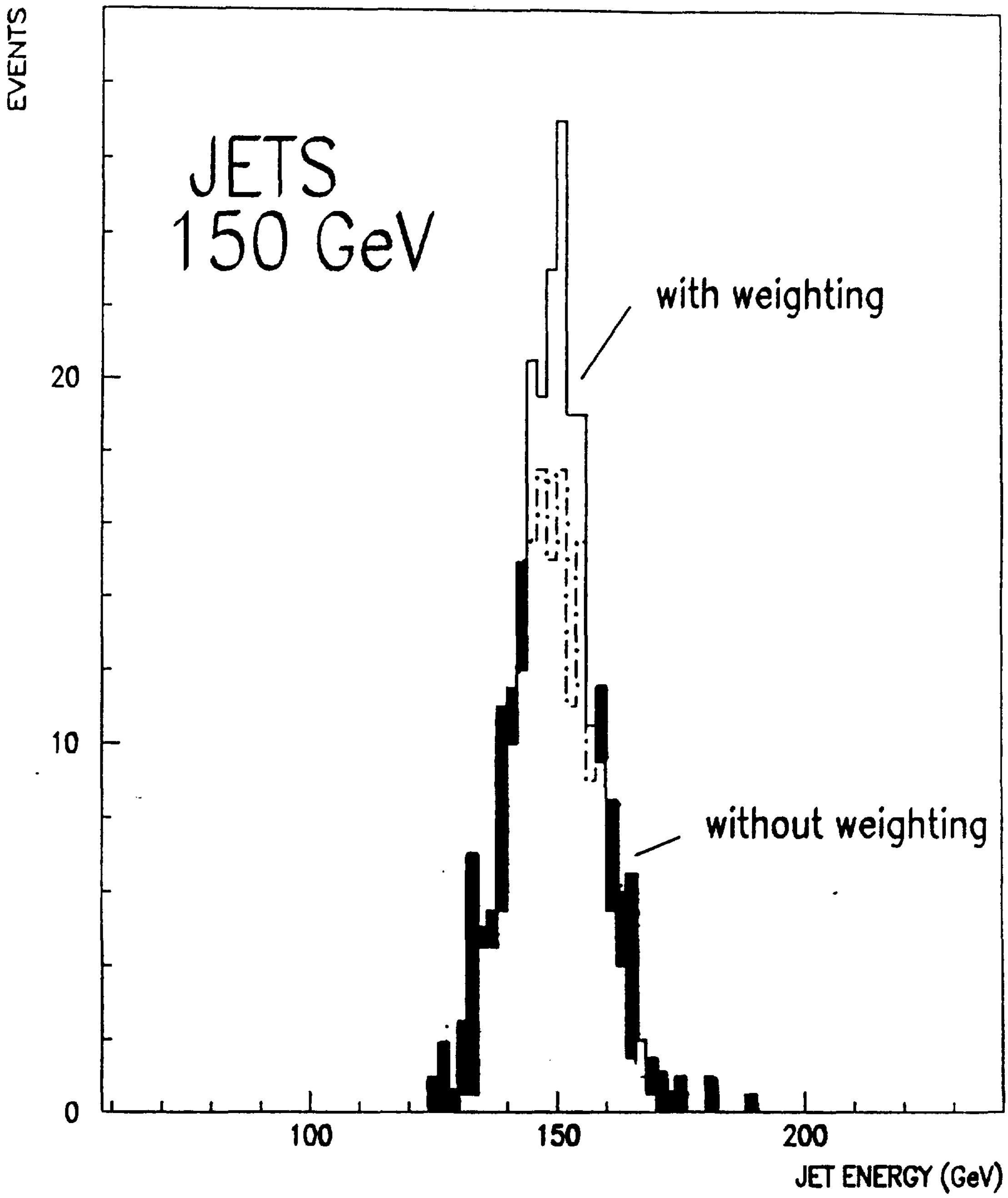

EVENTS
JETS
150 GeV
with weighting
without weighting
20
10
0
100
150
200
JET ENERGY (GeV)

Figure 1

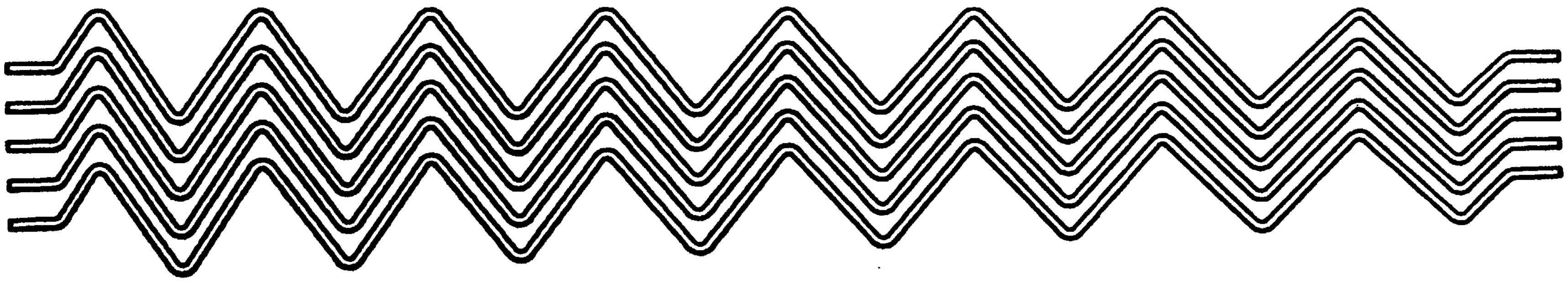

Figure 2

echelle: 1:2

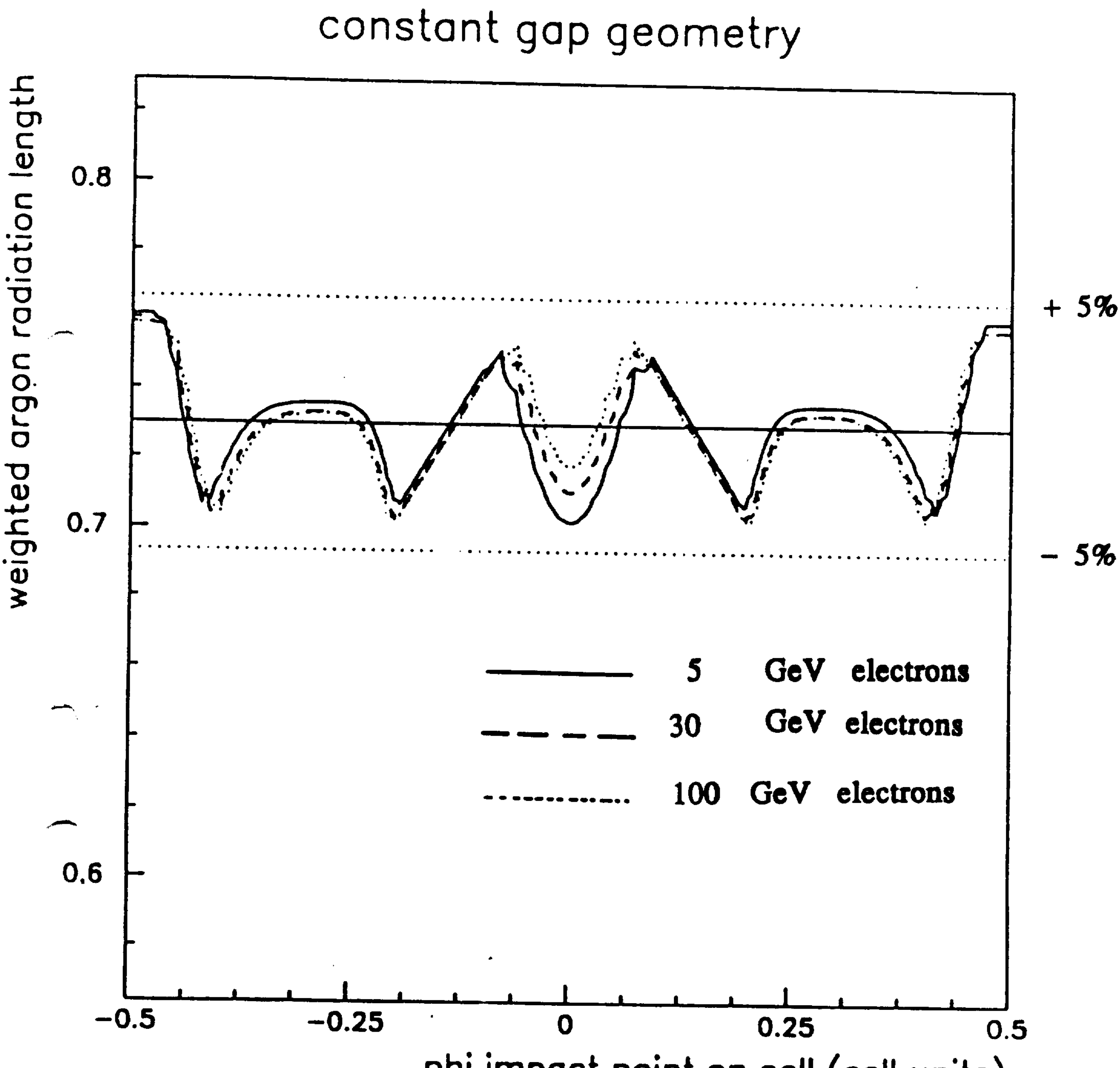

constant gap geometry
weighted argon radiation length
0.8
0.7
0.6
+ 5%
- 5%
5 GeV electrons
30 GeV electrons
100 GeV electrons
-0.5
-0.25
0
0.25
0.5
phi impact point on cell (cell units)

Figure 3

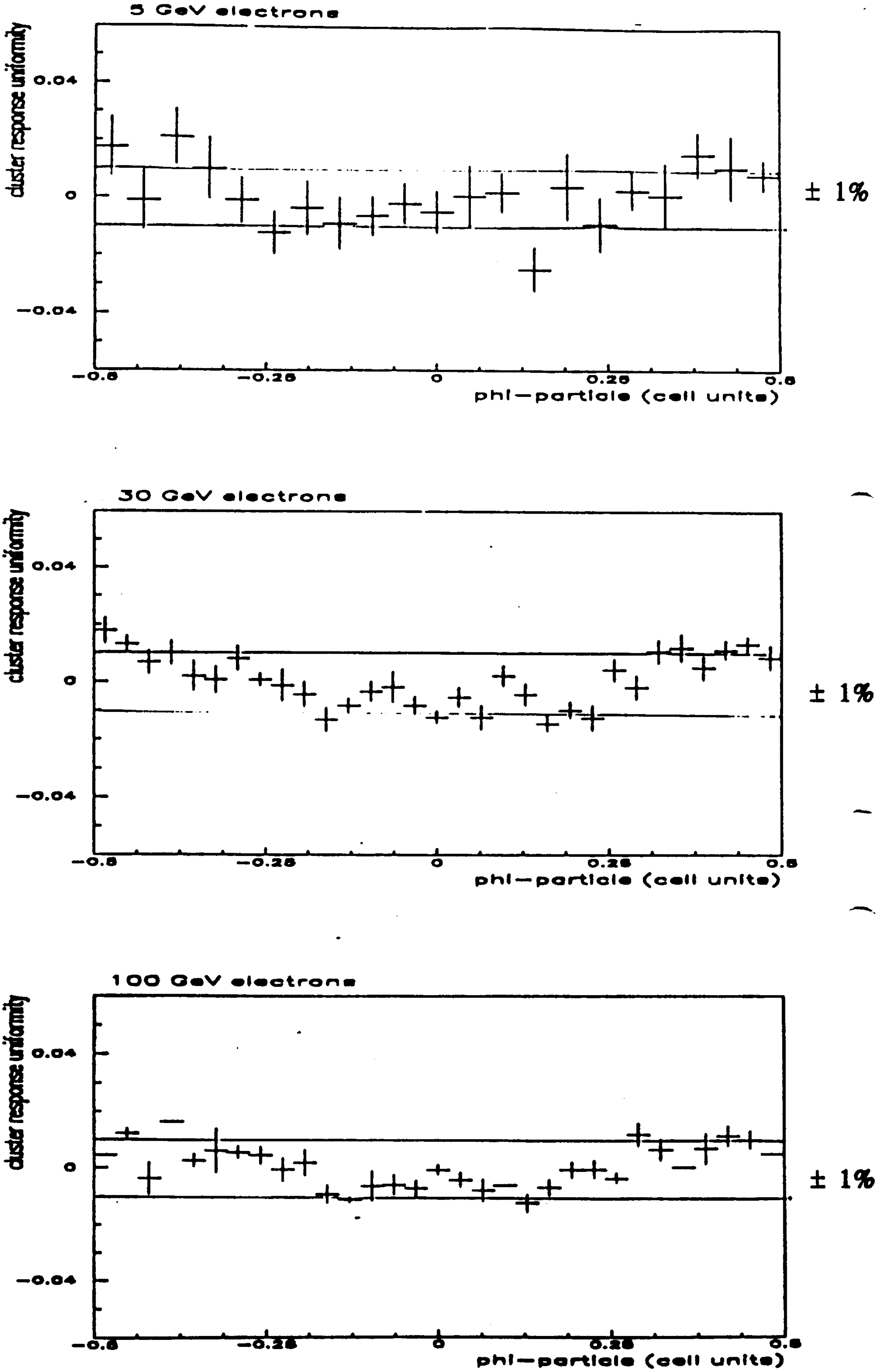
5 GeV electrons
cluster response uniformity
0.04
0
-0.04
-0.5
-0.25
0
0.25
0.5
phi-particle (cell units)
± 1%
30 GeV electrons
cluster response uniformity
0.04
0
-0.04
-0.5
-0.25
0
0.25
0.5
phi-particle (cell units)
± 1%
100 GeV electrons
cluster response uniformity
0.04
0
-0.04
-0.5
-0.25
0
0.25
0.5
phi-particle (cell units)
± 1%

Figure 4

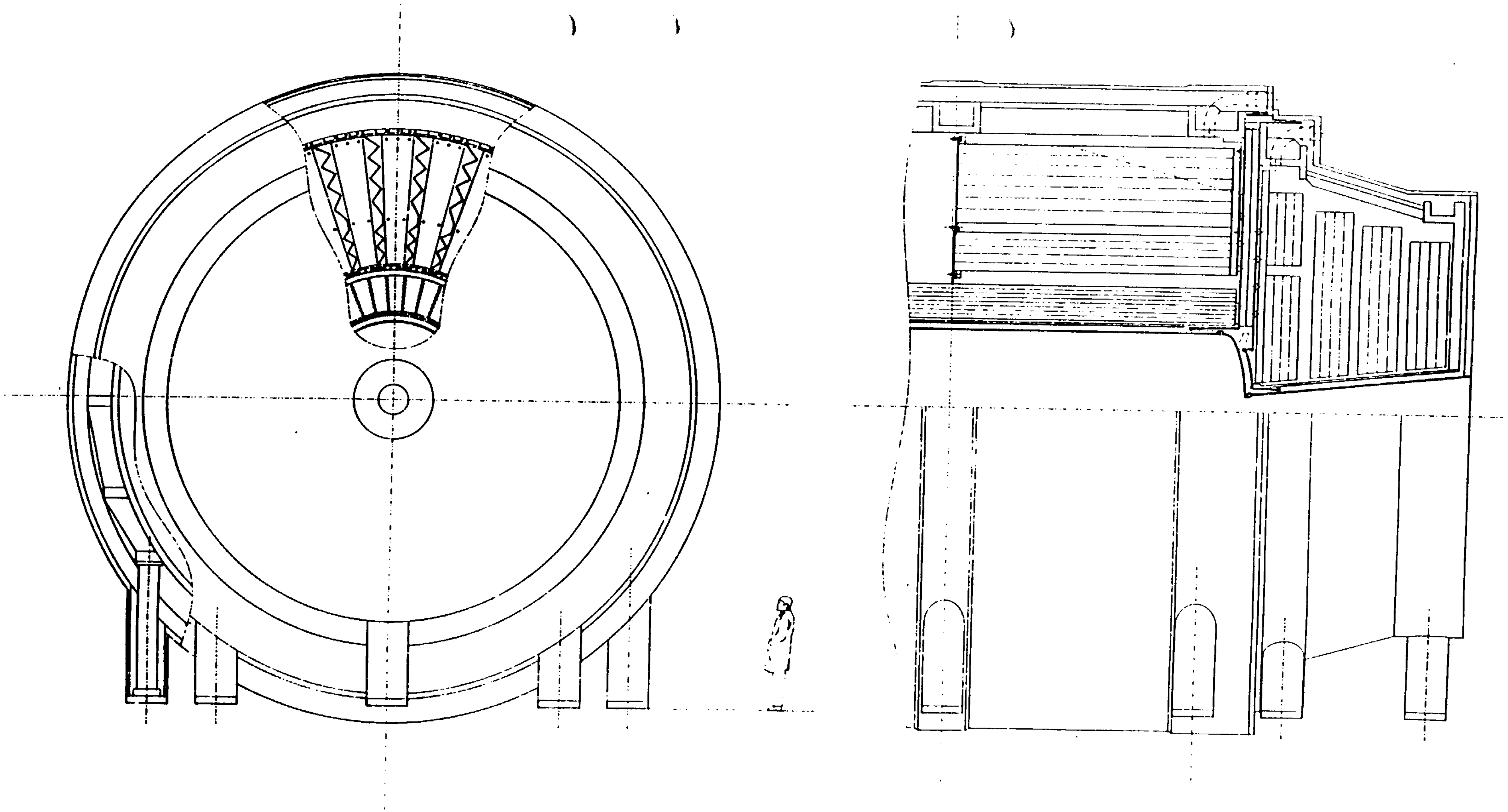

Figure 5

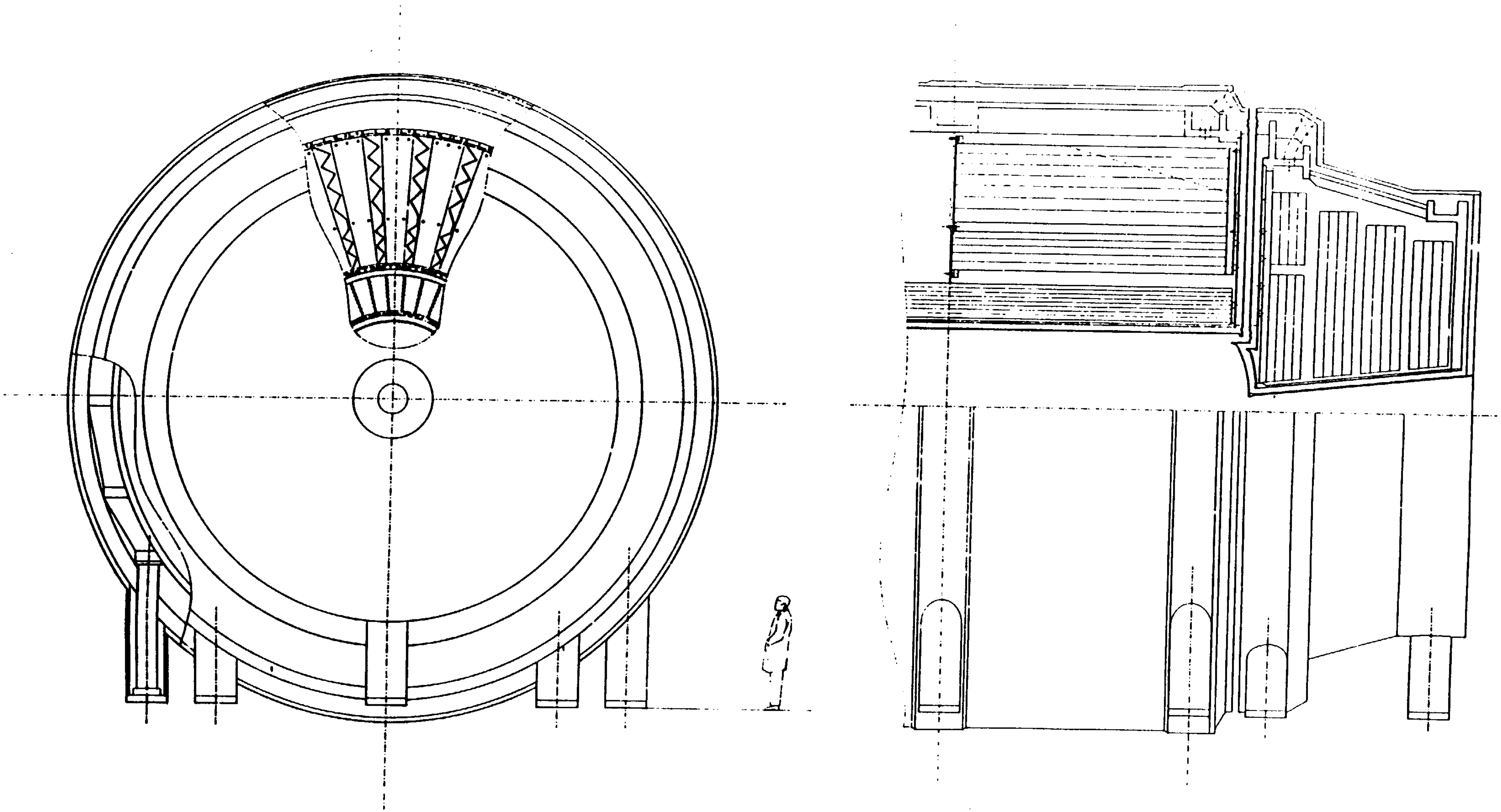

Figure 6

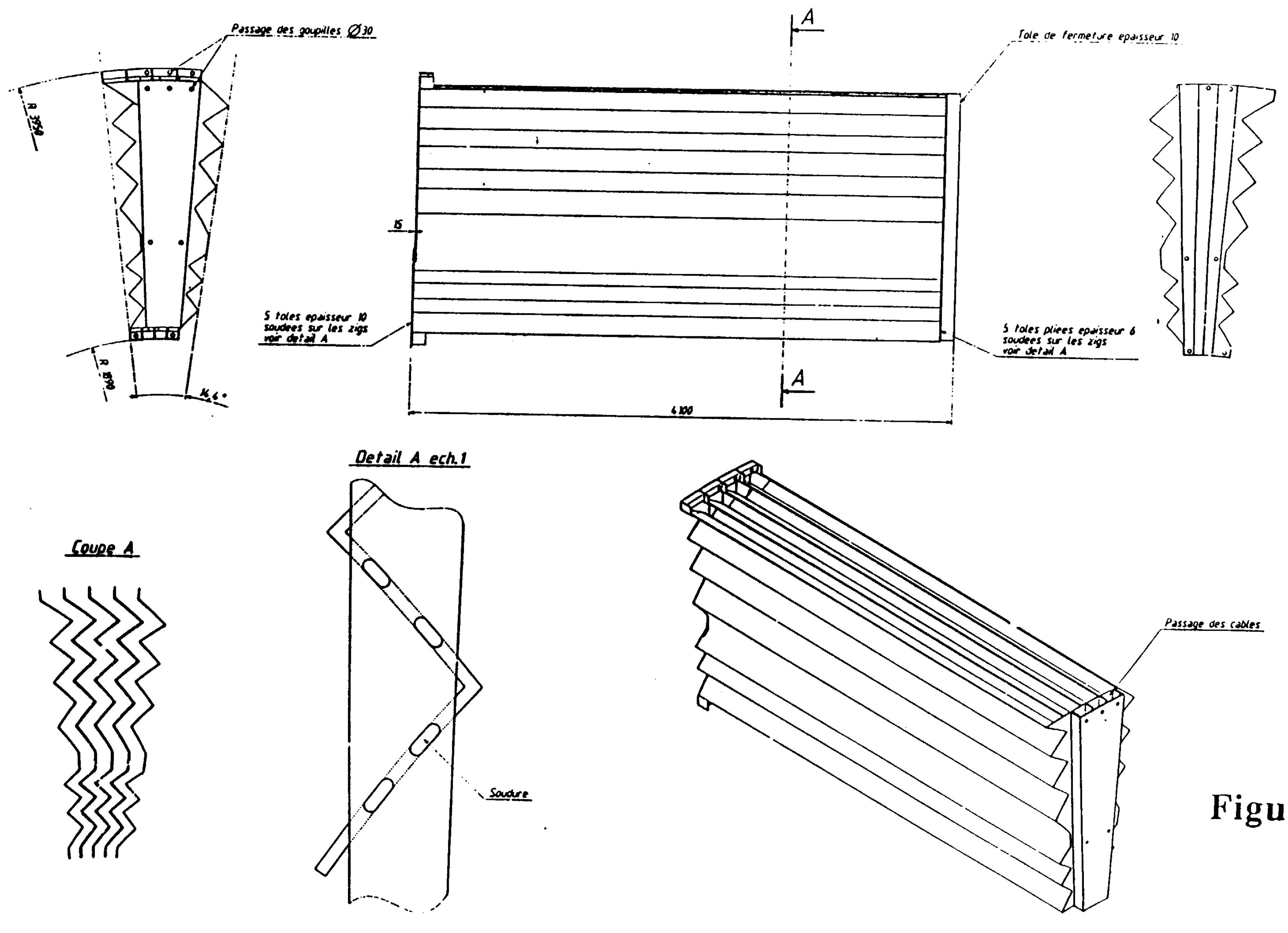
Passage des goupilles Ø30
R 3950
R 1590
14,6°
15
5 toles epaisseur 10
soudees sur les zigs
voir detail A
A
A
4100
Tole de fermeture epaisseur 10
5 toles pliees epaisseur 6
soudees sur les zigs
voir detail A
Coupe A
Detail A ech.1
Soudure
Passage des cables

Figure 7

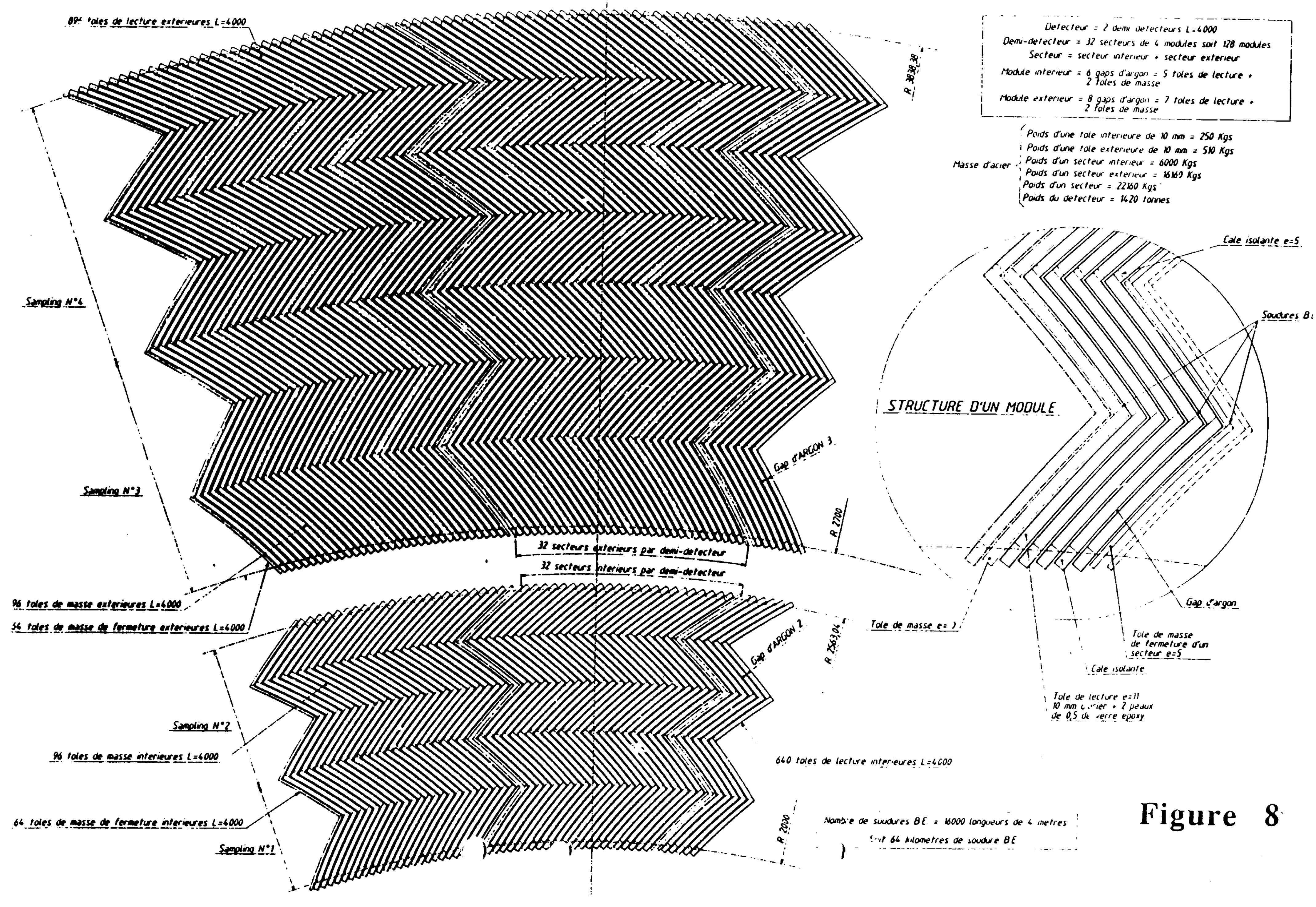

Detecteur = 2 demi detecteurs L=4000
Demi-detecteur = 32 secteurs de 4 modules soit 128 modules
Secteur = secteur interieur + secteur exterieur
Module interieur = 6 gaps d'argon = 5 toles de lecture + 2 toles de masse
Module exterieur = 8 gaps d'argon = 7 toles de lecture + 2 toles de masse
Masse d'acier
Poids d'une tole interieure de 10 mm = 250 Kgs
Poids d'une tole exterieure de 10 mm = 510 Kgs
Poids d'un secteur interieur = 6000 Kgs
Poids d'un secteur exterieur = 16160 Kgs
Poids d'un secteur = 22160 Kgs
Poids du detecteur = 1420 tonnes
STRUCTURE D'UN MODULE
Cale isolante e=5
Gap d'argon
Tole de masse de fermeture d'un secteur e=5
Cale isolante
Tole de masse e=
89 toles de lecture exterieures L=4000
R 3838,38
Sampling N°4
Sampling N°3
Gap d'ARGON 3
R 2700
32 secteurs exterieurs par demi-detecteur
32 secteurs interieurs par demi-detecteur
96 toles de masse exterieures L=4000
54 toles de masse de fermeture exterieures L=4000
Gap d'ARGON 2
R 2563,04
Sampling N°2
96 toles de masse interieures L=4000
640 toles de lecture interieures L=4000
64 toles de masse de fermeture interieures L=4000
Sampling N°1
R 2000
Nombre de soudures BE = 16000 longueurs de 4 metres
64 kilometres de soudure BE

Figure 8

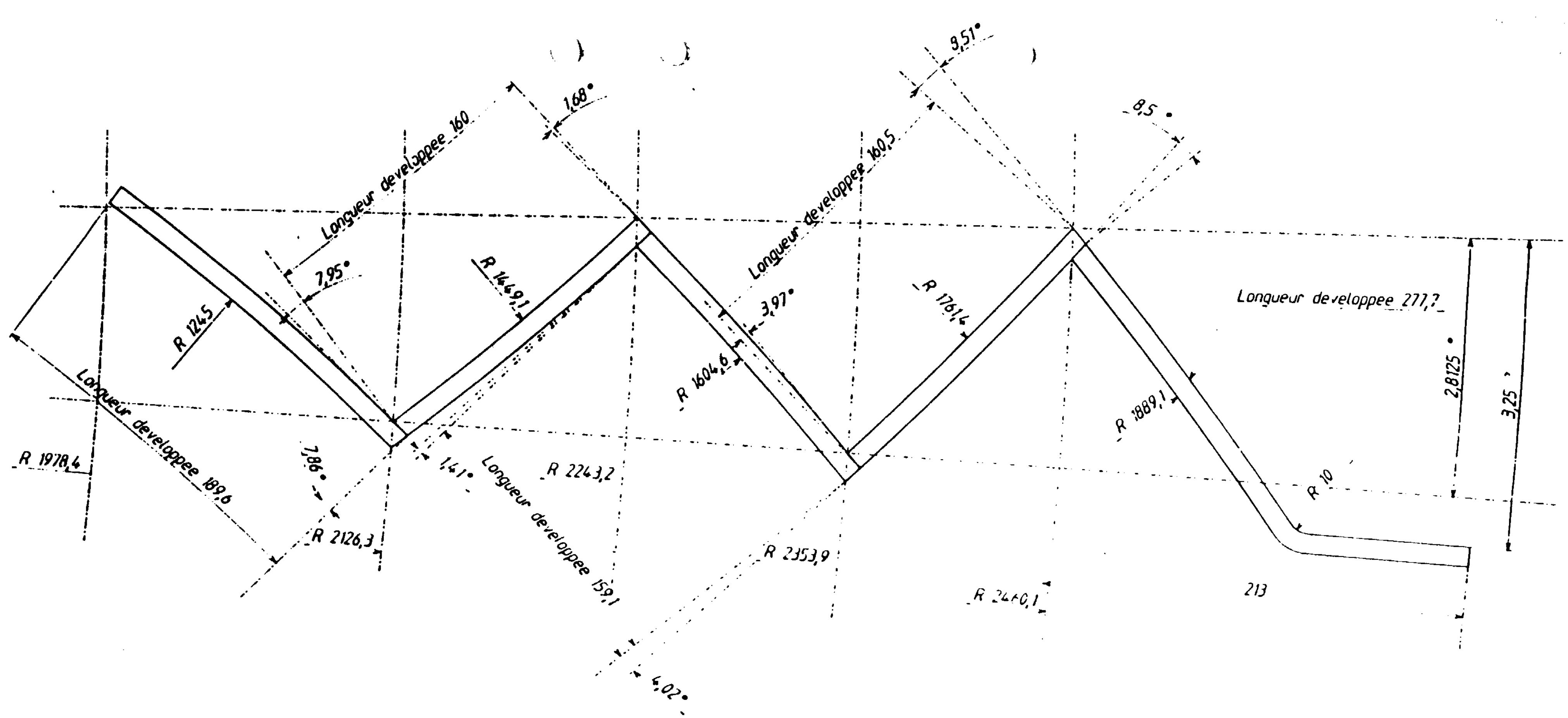

Epaisseur des toles 10 mm

Longueur des toles 4000

Figure 9

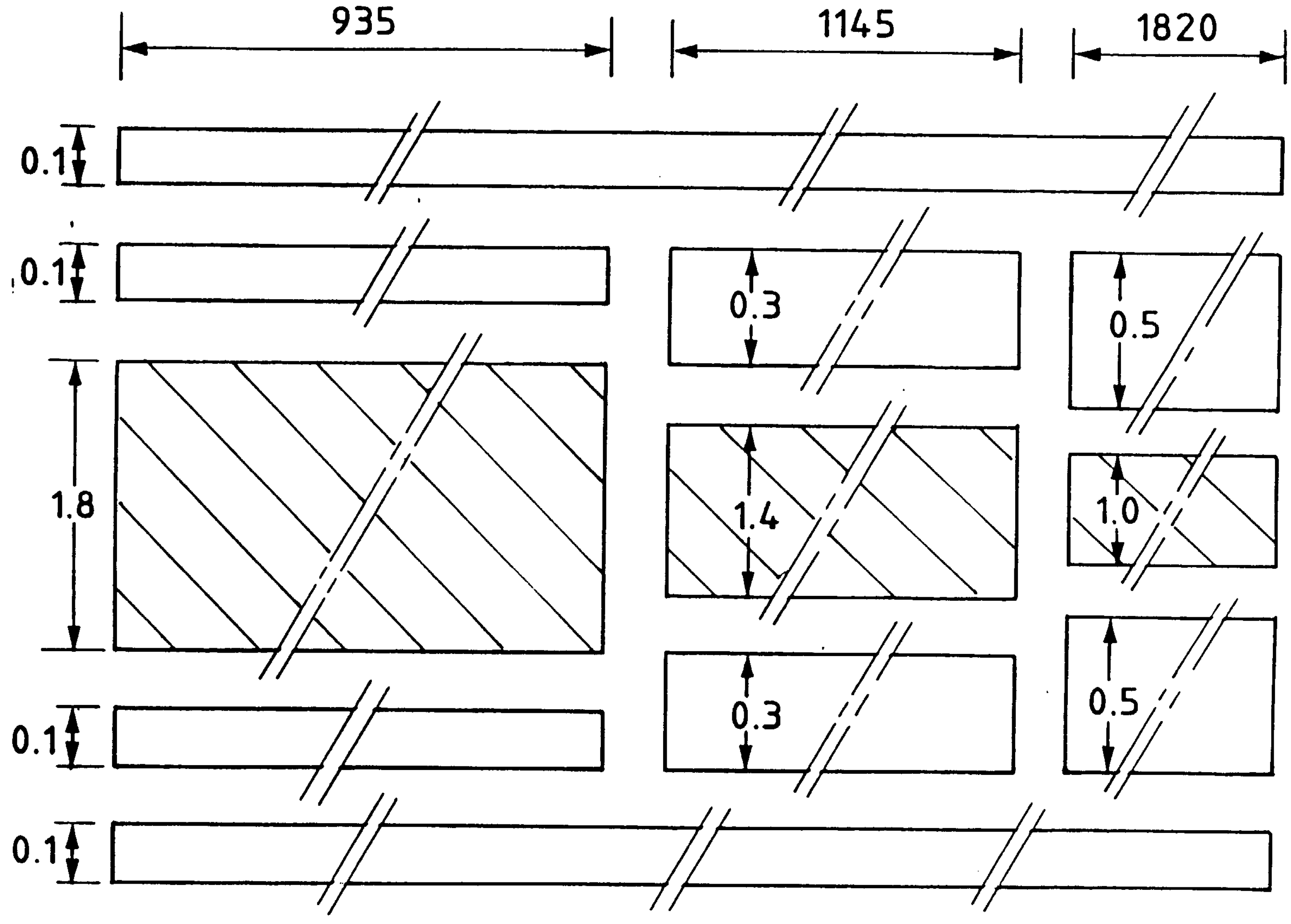

Figure 10

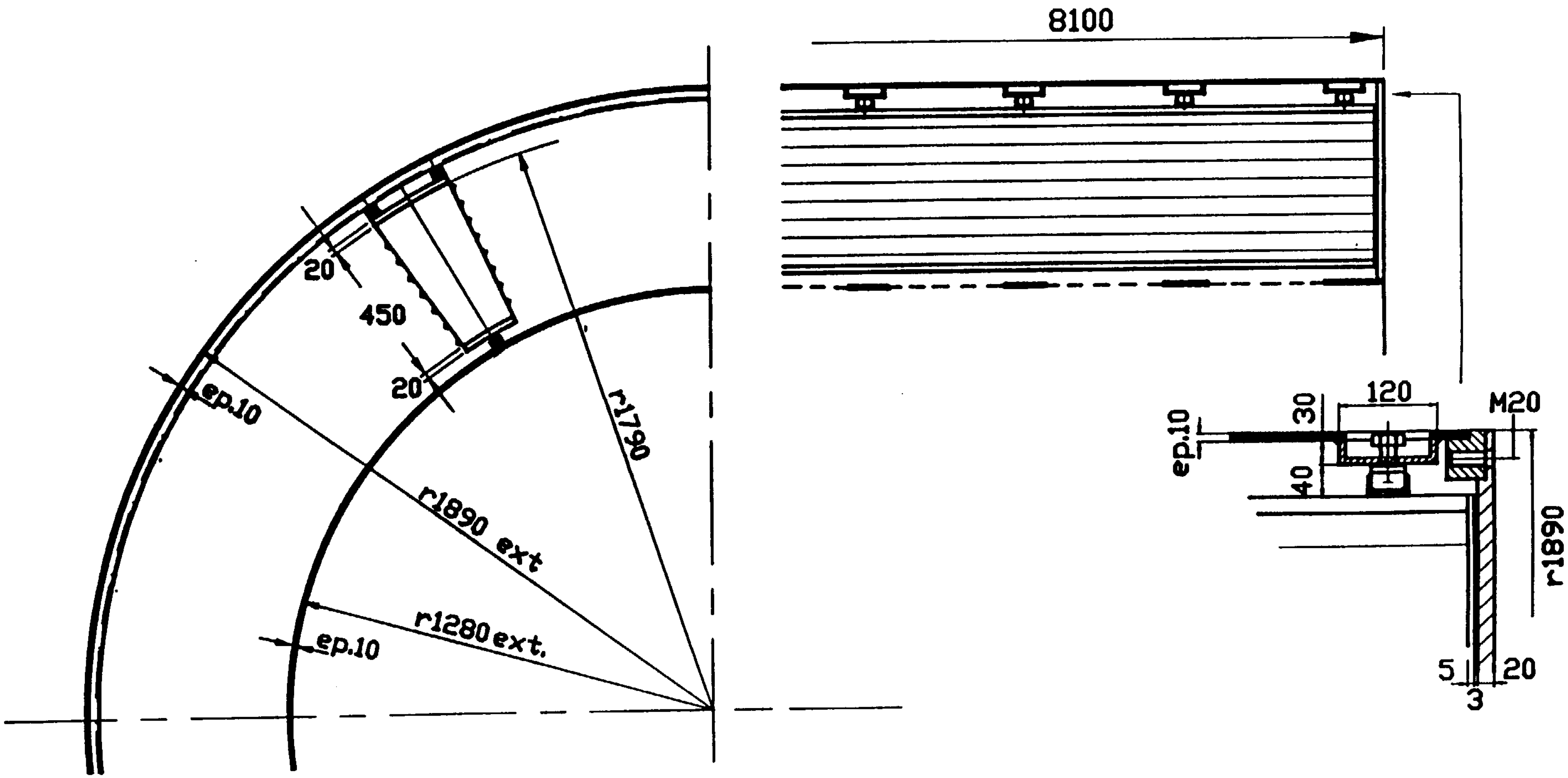
8100
20
450
20
ep.10
r1790
r1890 ext
r1280 ext.
ep.10
120
30
M20
ep.10
40
r1890
5
20
3

Figure 11

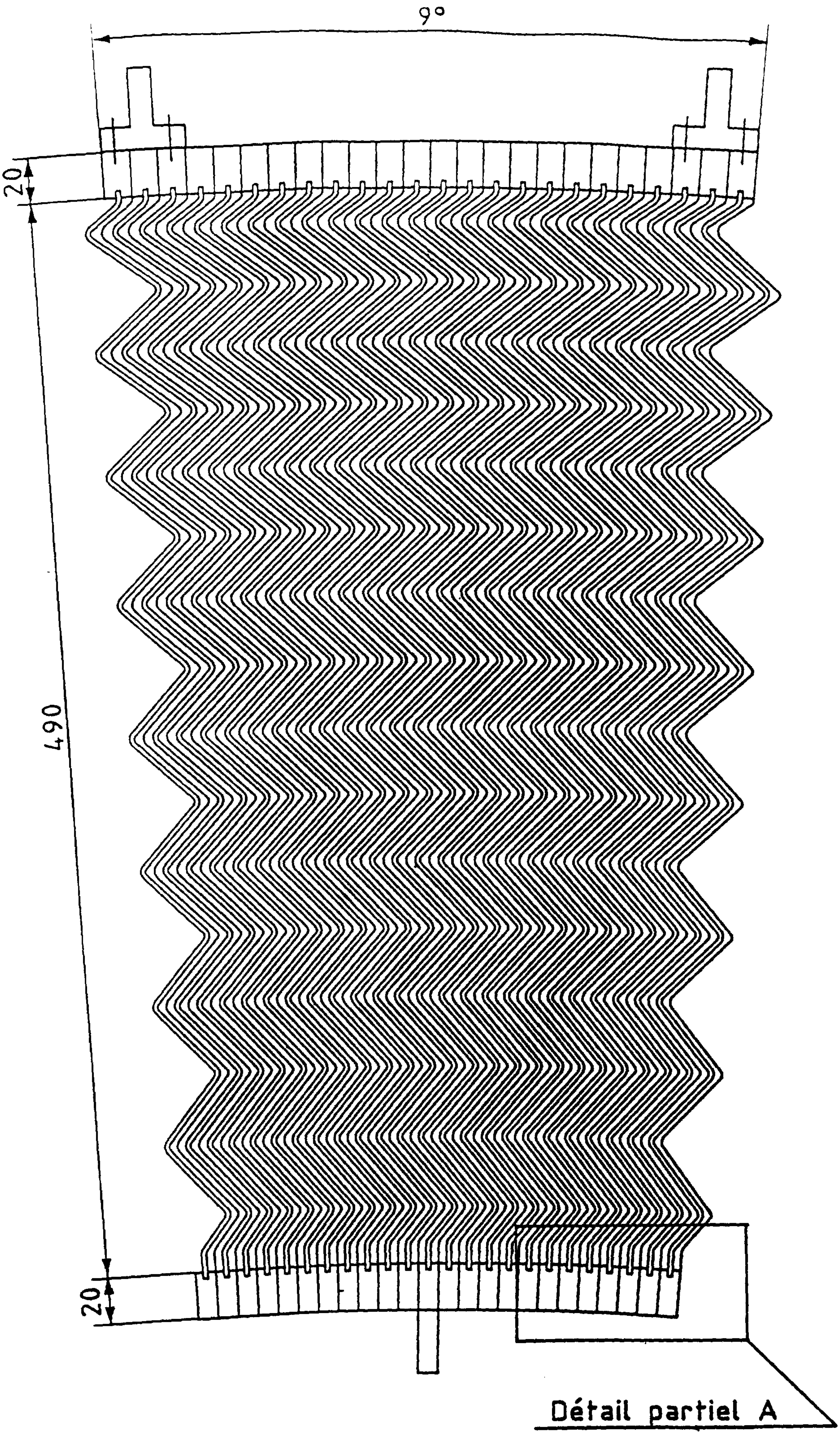

Figure 12

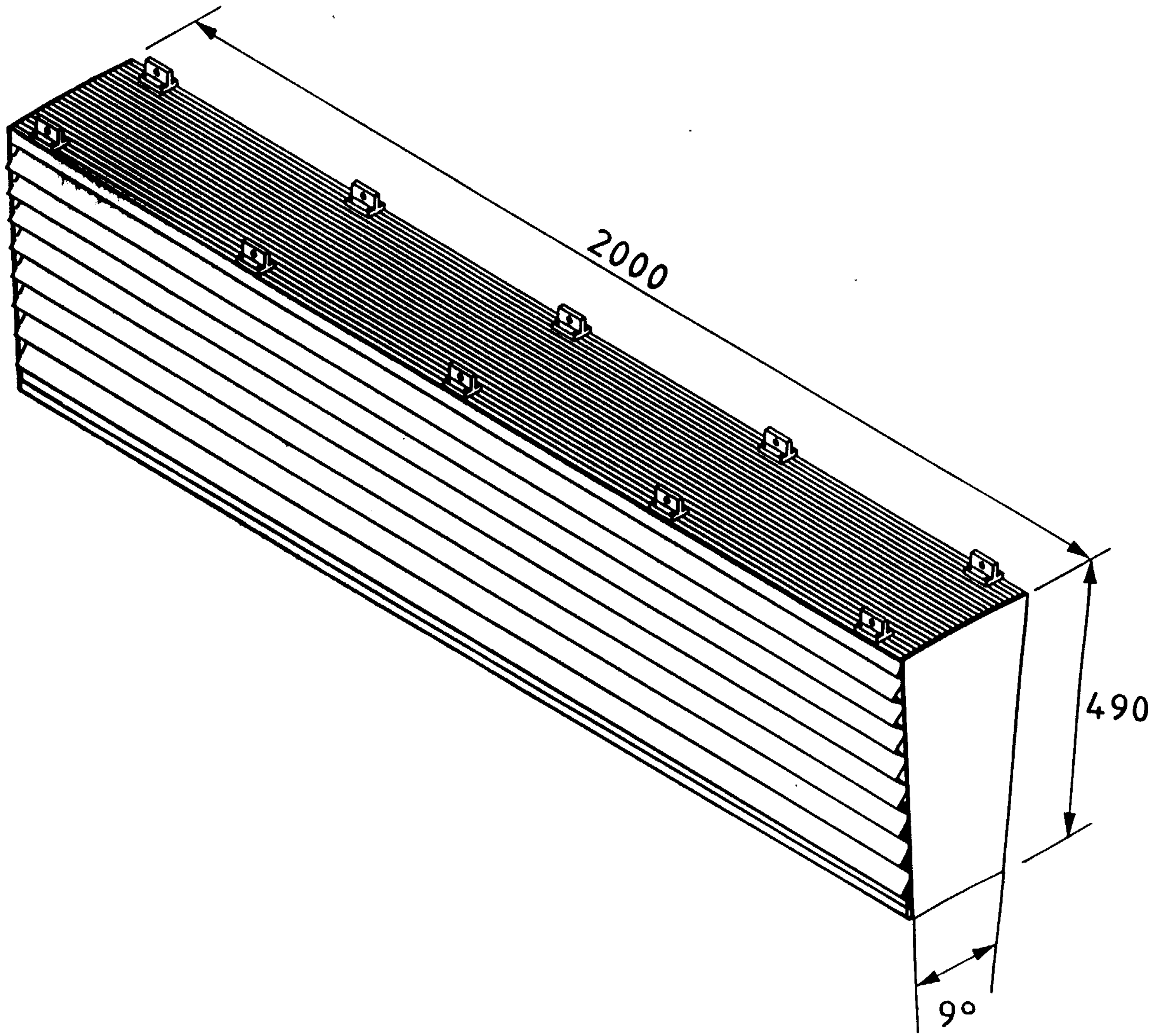

Figure 13

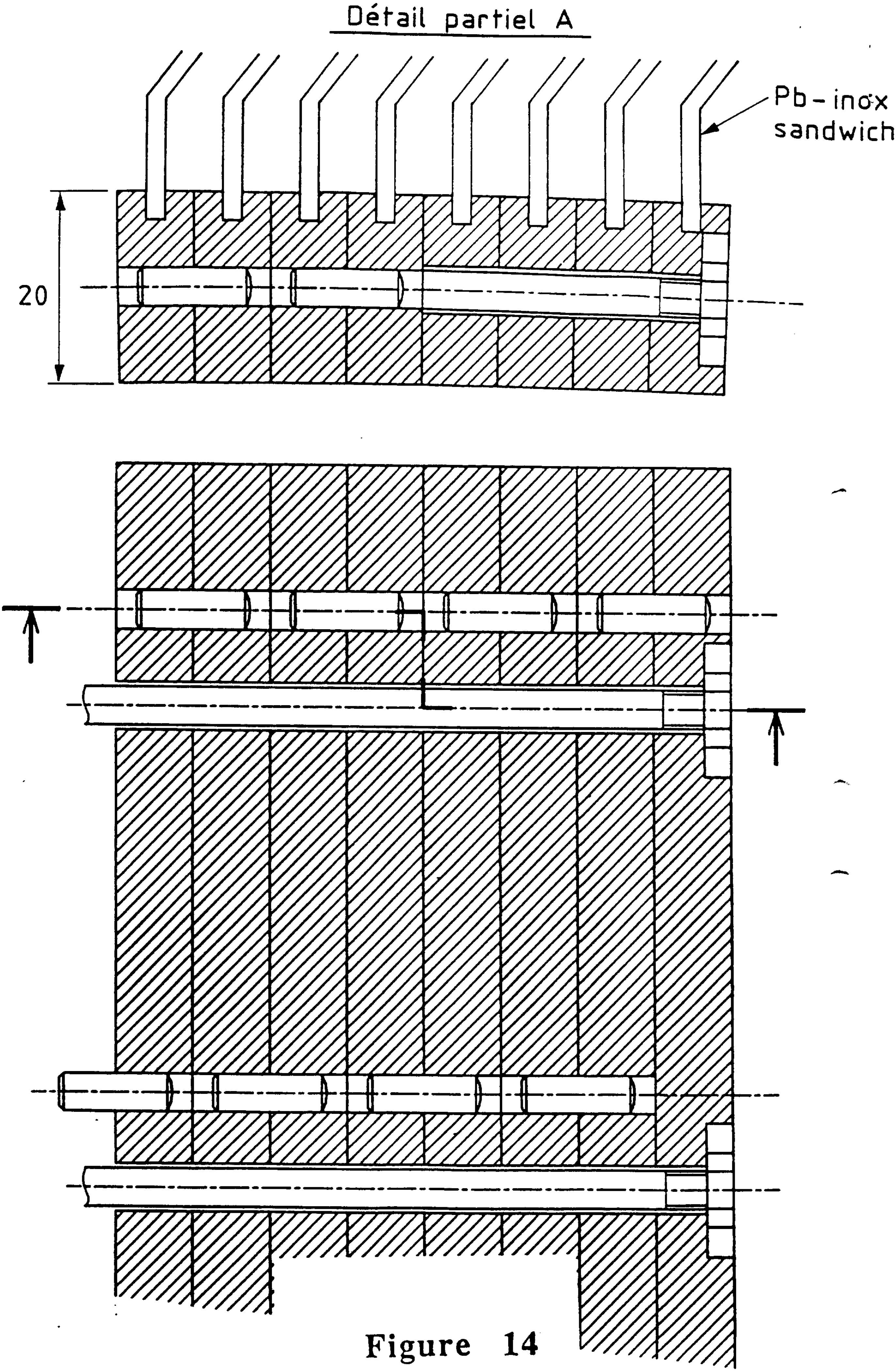

Figure 14

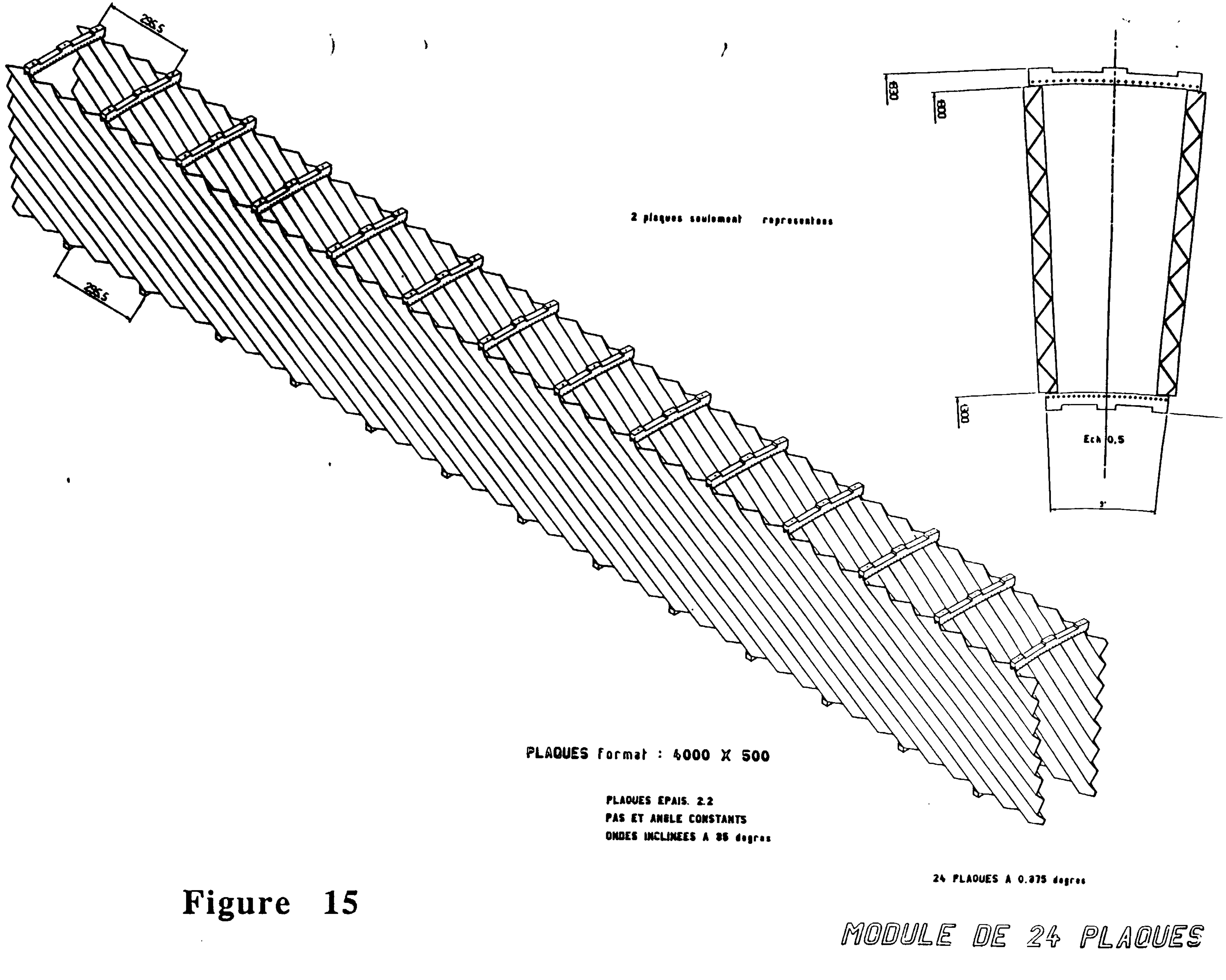
295.5
295.5
2 plaques seulement representees
1830
1800
1300
Ech 0,5
3°
PLAQUES format : 4000 X 500
PLAQUES EPAIS. 2.2
PAS ET ANGLE CONSTANTS
ONDES INCLINEES A 35 degres
24 PLAQUES A 0.375 degres
MODULE DE 24 PLAQUES

Figure 15

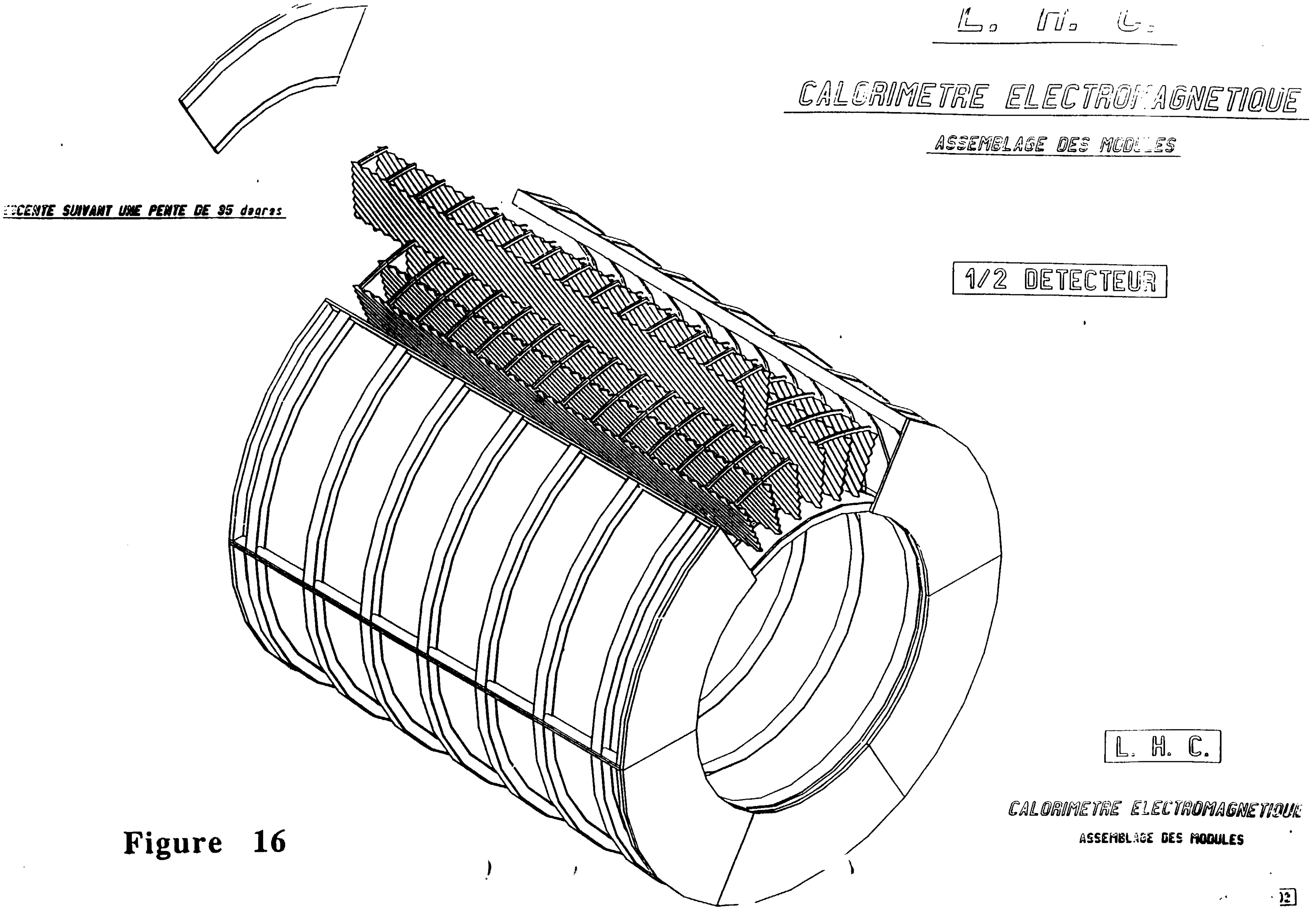
L. H. C.
CALORIMETRE ELECTROMAGNETIQUE
ASSEMBLAGE DES MODULES
DESCENTE SUIVANT UNE PENTE DE 95 degres
1/2 DETECTEUR
L. H. C.
CALORIMETRE ELECTROMAGNETIQUE
ASSEMBLAGE DES MODULES

Figure 16

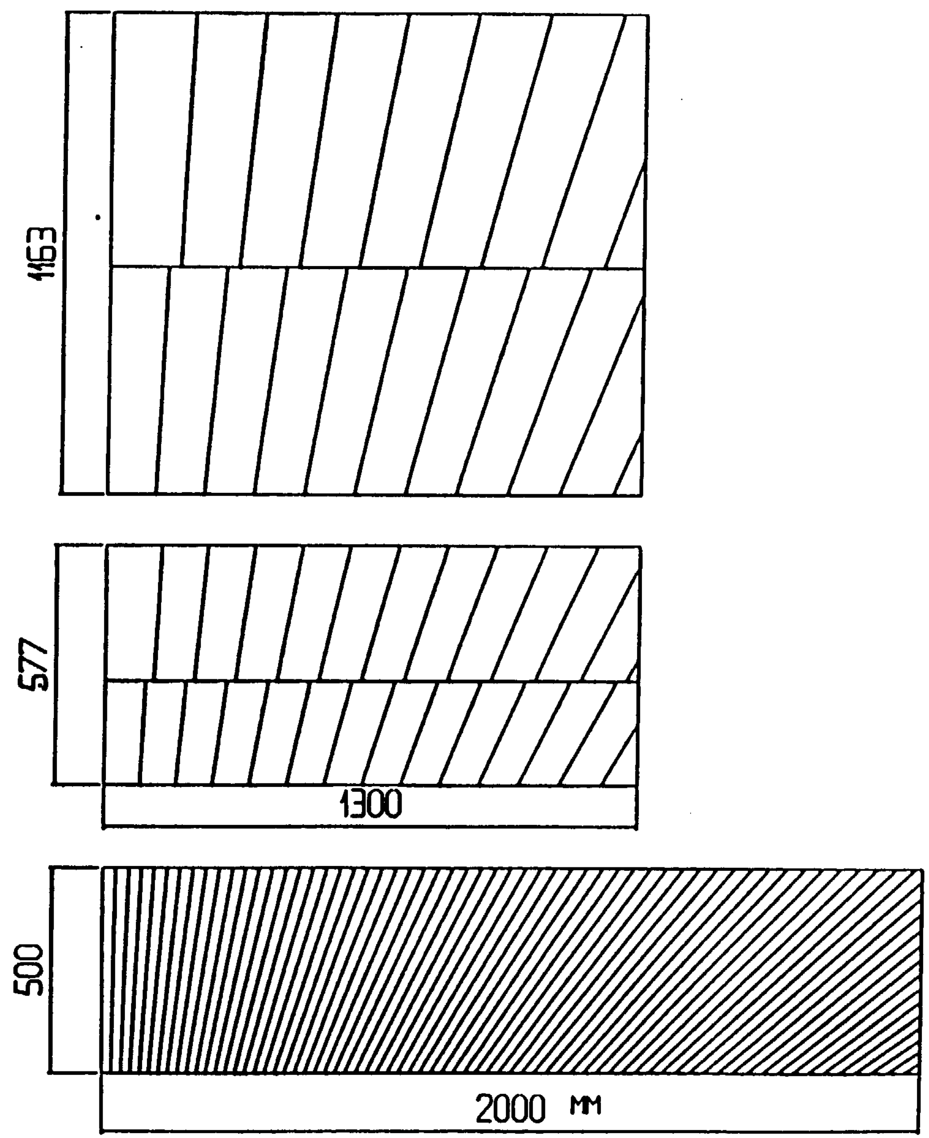

Figure 17

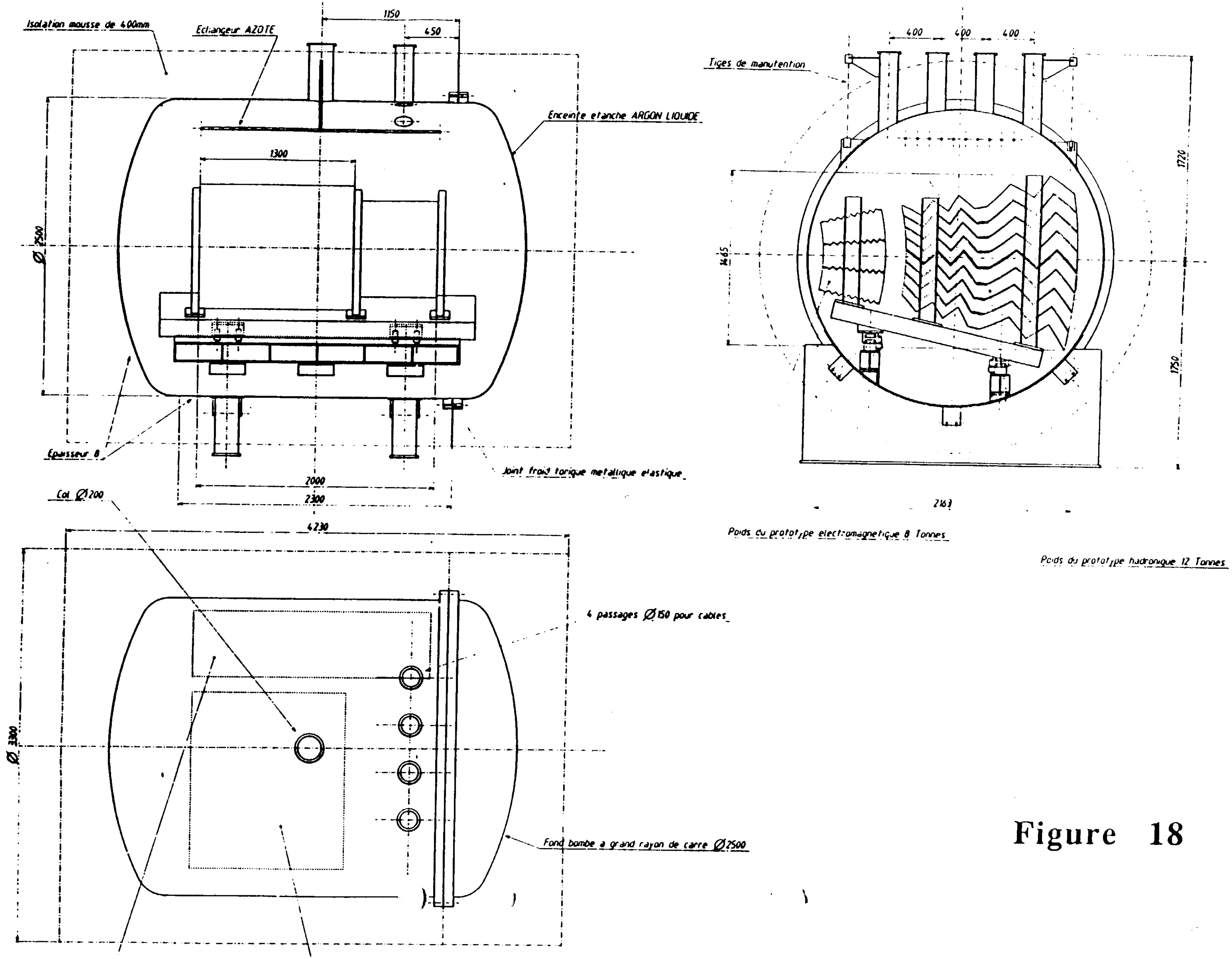
Isolation mousse de 400mm
Echangeur AZOTE
1150
450
Enceinte etanche ARGON LIQUIDE
1300
Ø 2500
Epaisseur 8
Joint froid torique metallique elastique
2000
2300
Col Ø200
4230
4 passages Ø150 pour cables
Ø 3300
Fond bombe a grand rayon de carre Ø2500
400
400
400
Tiges de manutention
1720
1465
1750
2163
Poids du prototype electromagnetique 8 Tonnes
Poids du prototype hadronique 12 Tonnes

Figure 18

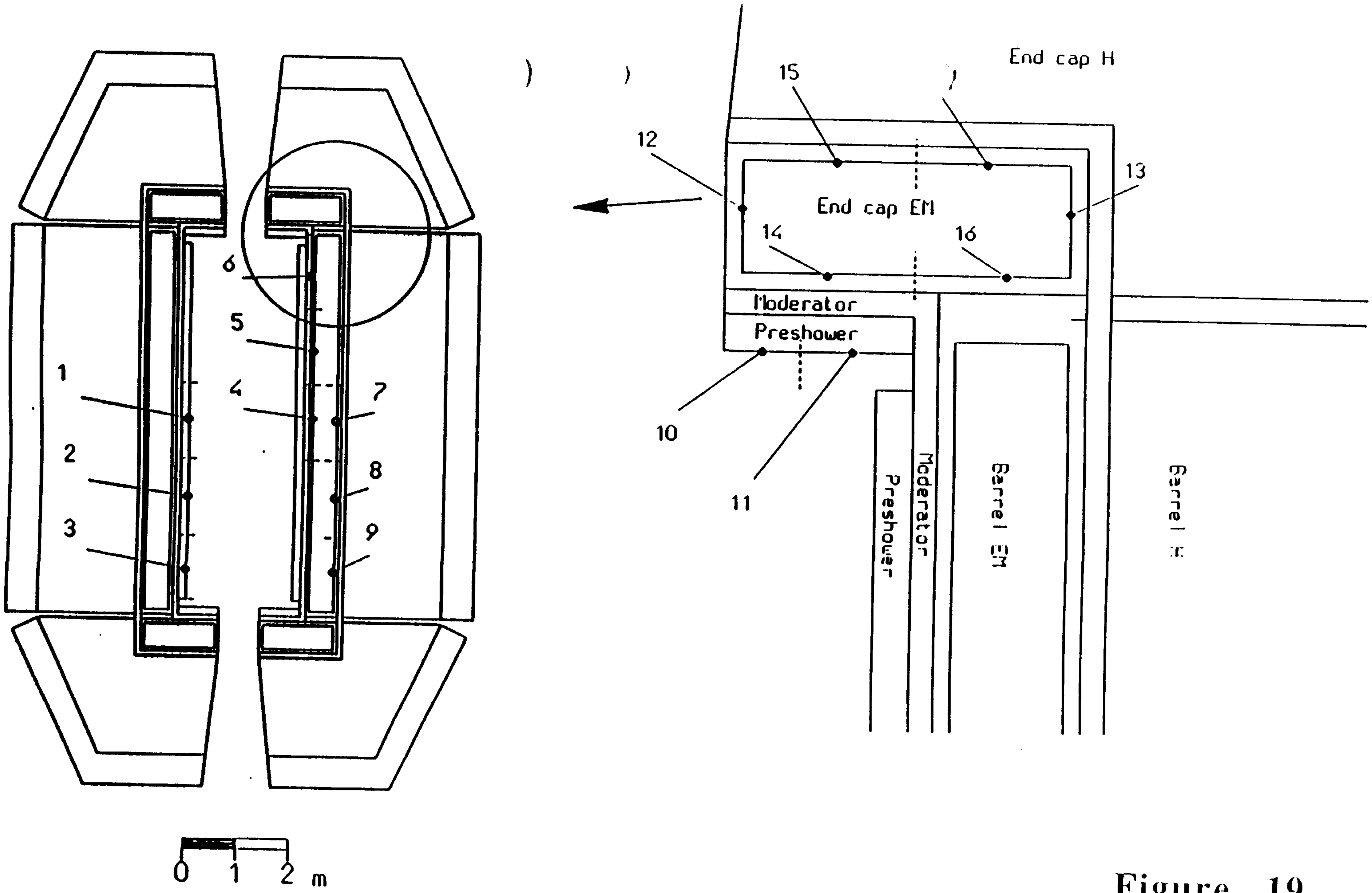
1
2
3
4
5
6
7
8
9
0 1 2 m
12
15
13
14
16
10
11
End cap H
End cap EM
Moderator
Preshower
Barrel EM
Barrel H

Figure 19

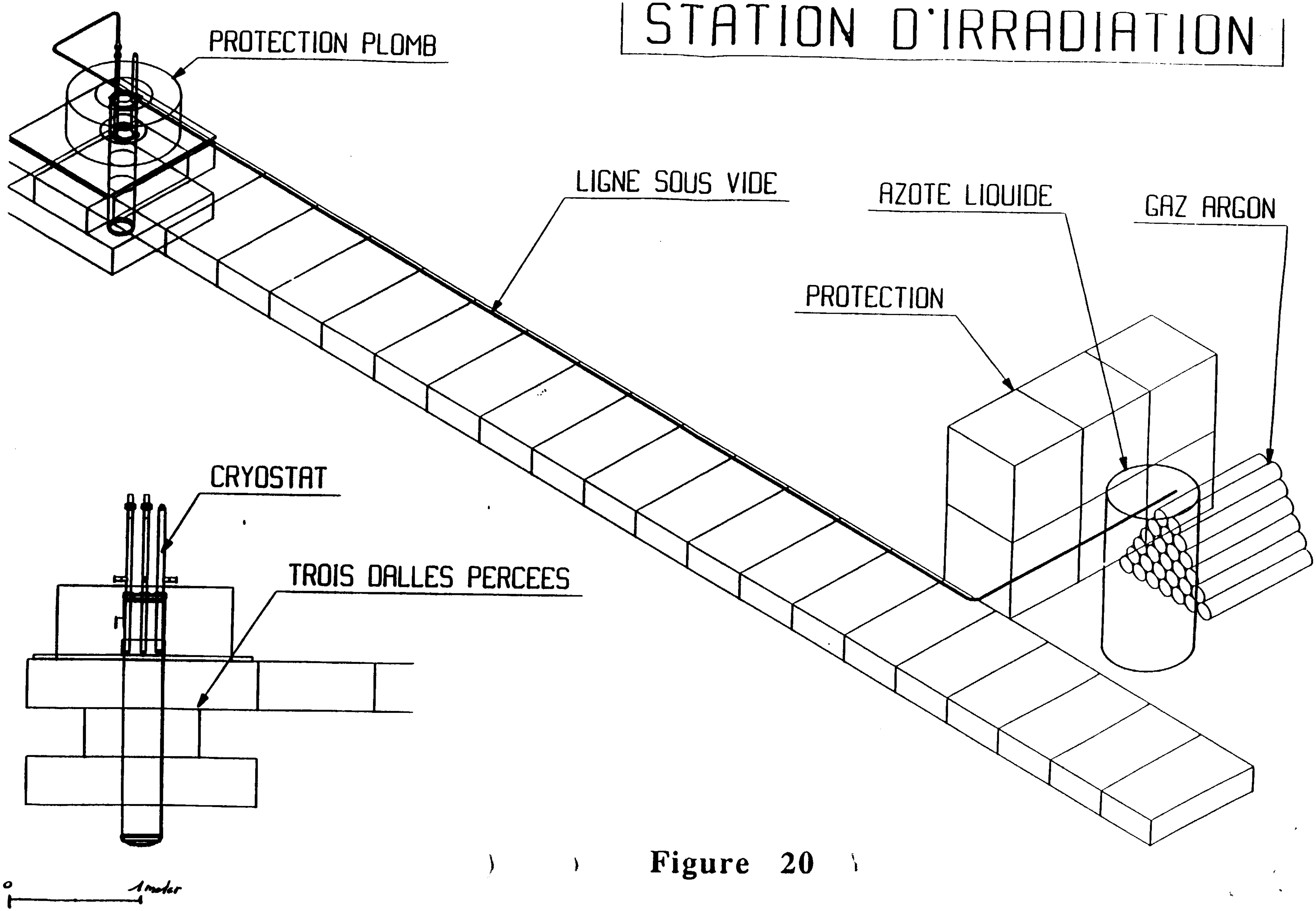
STATION D'IRRADIATION
PROTECTION PLOMB
LIGNE SOUS VIDE
AZOTE LIQUIDE
GAZ ARGON
PROTECTION
CRYOSTAT
TROIS DALLES PERCEES
0
1 metre

Figure 20